Adsorptive Removal of Manganese Ions From Polluted Aqueous Media by Glauconite Clay-Functionalized Chitosan Nanocomposites: Adsorption, Kinetic, Isotherm, and Thermodynamic Investigations

Mostafa Y Nassar (m_y_nassar@yahoo.com)
Ain Shams University https://orcid.org/0000-0002-5177-9777
Marwa M. Sobeih
Ain Shams University
M.F. El-Shahat
Ain Shams University
A. Osman
Ain Shams University
M. A. Zaid
Ain Shams University

Research Article

Keywords: Manganese ions, adsorptive removal, glauconite clay, functionalized chitosan nanocomposite

Posted Date: March 22nd, 2021

DOI: https://doi.org/10.21203/rs.3.rs-322618/v1

Adsorptive removal of manganese ions from polluted aqueous media by glauconite clay-functionalized chitosan nanocomposites: Adsorption, kinetic, isotherm, and thermodynamic investigations

Marwa M. Sobeih [1,2], M.F. El-Shahat[1]*, A. Osman[3], M. A. Zaid[2], Mostafa Y. Nassar[4]*

[1]Chemistry Department, Faculty of Science, Ain Shams University, Cairo, Egypt

[2]Abu-Zaabal Company for Fertilizer and Chemical Company (AZFC), EL-Qalyubia, Egypt

[3]Geology Department, Faculty of Science, Ain Shams University, Cairo, Egypt

[4]Chemistry Department, Faculty of Science, Benha University, Benha 13815, Egypt

*Corresponding authors: E-mail address: m_y_nassar@yahoo.com, m_y_nassar@fsc.bu.edu.eg. Tel.: +20 1068727555 (M.Y. Nassar). elshahatmf@hotmail.com, Tel.: +20 1128323115 (M.F. El-Shahat). Marwa_Sobeih1@yahoo.com, Tel.: +01093279991 (M.M. Sobeih).

Abstract

The presence of Mn(II) in water exceeding the permitted concentration declared by the World Health Organization (WHO) influences individuals, animals, and the ecosystem negatively. Therefore, there is a necessity for an efficient material to eliminate this potentially toxic element from wastewater. We herein focused on an adsorptive removal of Mn(II) ions from polluted aqueous media using natural Egyptian glauconite clay (G) and its nanocomposites with a modified chitosan (CS). The applied chitosan was modified with glutaraldehyde (GL), ethylenediaminetetraacetic acid (EDTA), sodium dodecyl sulfate (SDS) and cetyltrimethyl

ammonium bromide (CTAB). The utilized nanocomposites were referred to as GL-CS/G, EDTA-GL-CS/G, SDS-CS/G, and CTAB-CS/G, respectively. The points of zero charge values of the as-prepared materials were estimated. The adsorption properties of the G clay and its nanocomposites toward the removal of Mn(II) ions from polluted aqueous media as well as the adsorption mechanism were explored using a batch technique. The glauconite (G) and its nanocomposites: GL-CS/G, CTAB-CS/G, EDTA-GL-CS/G, and SDS-CS/G, exhibited maximum adsorption capacity values of 3.750, 24.11, 26.25, 27.15, and 27.74mgg^{-1}, respectively. The adsorption results fitted well the Langmuir isotherm and pseudo-second-order kinetic models. The determined thermodynamic parameters revealed that the Mn(II) ion adsorption process was endothermic, spontaneous, and physisorption controlled. Furthermore, the obtained adsorption results are encouraging and revealing a great potentiality for using the modified adsorbents as accessible adsorbents for Mn(II) ions removal from polluted aqueous solutions, depending on their reusability, high stability and good adsorption capacities.

Keywords: Manganese ions; adsorptive removal; glauconite clay; functionalized chitosan nanocomposite.

1- Introduction

Heavy metals are considered one of the main sources of industrial wastewater pollution, which seriously menace the human health and the biological environment. It is necessary to remove the inorganic pollutants from wastewater before being discharged into the environment due to their high stability and non-degradable nature (1, 2). Although some heavy metals such as manganese, copper, iron, and zinc are essential for human health under particular concentrations, but above these concentrations they become toxic and cause various health problems (3). Water

contamination with heavy metals such as manganese is a problematic problem, and it has attracted significant interest from many research groups (3, 4). Manganese is one of those inorganic pollutants present in aquatic environment. It has three possible oxidation states, namely Mn(II), Mn(III) and Mn(IV). The Mn(II) ion is the only form that is stable in soil solution, whereas Mn(III) and Mn(IV) forms are only stable in the solid phase. The divalent manganese (Mn(II)) is discharged via the wastewaters of ceramics, battery, electrical coils, glass, leather, and textile industries (5). As mentioned before, trace amounts of manganese ions are useful for human body, since they act as an activator for some enzymes (6). However, high concentrations of manganese ions can cause various health diseases such as cells mutation, damage of central nervous systems, weakness, lack of fertility, acute intoxication, permanent disabilityand paralysis (7).Therefore, the recommended levels permitted for manganese concentrations are 0.05 mgL^{-1} in drinking water and 5.0 mg/L in surface water according to the drinking water quality standard and the recommendations of USEPA (8). Hence, the removal of Mn(II) ions from wastewater is necessary for human and environmental safety.

To date, different techniques have been developed for manganese ions removal from aqueous solutions such as ion-exchange, precipitation, membrane filtration, bio- degradation, solvent extraction, and advanced oxidation, and adsorption (9). However, due to simplicity, high efficiency, low-cost and wide adaptability of the adsorption process, it still has the superiority among other techniques (10, 11). In this context, various adsorbent materials, including clay minerals, natural and prepared polymers, activated carbons, zeolites, and agricultural byproducts have been used for manganese ions removal from wastewater (12). use of clays as adsorbent to remove Mn(II) from water has great advantages compared with other commercial adsorbents in terms of high specific surface area, low-cost, high adsorption properties, availability, non-toxicity

and large potential for ion exchange (13). In this light,one of natural clay minerals known as glauconite clay (G) was selected for Mn(II) ions adsorption. Glauconite like other clay mineral characterized by chemical and mechanical stability, layered structure, large surface area as well as high thermal stability and little electrical conductivity due to the existence of metal oxides in its composition (14). Its structure is classified as 2:1 type with presence of one octahedral sheet sandwiched by two tetrahedral sheets (15). It has a chemical formula of (K, Na) (Fe, Al, $Mg)_2$ $(Si, Al)_4$ $O_{10}(OH)_2$, with presence of two types of iron (Fe^{2+} and Fe^{3+}) ions. The content of Fe^{3+} cations may be accountable for its properties as it is usually found in an amount greater than Fe^{2+} (16). Despite, G exhibits strong adsorption property that can be employed as cation exchanger and as an effective absorber in water and oil products (16), it have poor sedimentation properties, which can be overcome by using coagulants or applying a relatively long stability time, which in turn considered an additional cost of the overall operation (17). Therefore, various modification process chemical or physical can be undertaken for improving their removal efficiency (18).

Recently, the modification of clays by natural or synthetic polymers has gained critical research interest producing new compounds containing both organic and inorganic ingredients with distinguishable interface and diverse chemical and physical characteristics, such as corrosion resistance, low density, thermal isolation, high hardiness and flame retardants (19). Among all the most common polymers, chitosan is the second-most abundant natural biopolymer with distinct advantages. Chitosan gained interest of scientists not only owing to it's astonishing properties like local availability, biocompatibility, biodegradability, non-toxicity, low cost, bioactivity, attractive physical and mechanical properties, besides a presence of large number of amine and hydroxyl functional groups (20), but also due to its simplicity for development as a multifunctional

adsorbent depending upon the applied field. Chitosan is a cationic polymer resulting from N-deacetylation of chitin in alkaline medium (21). Due to the solubility of chitosan in dilute mineral acids, its chemical stability should be enhanced by special modification. Most of these methods are done using functional crosslinking agents, which unfortunately can reduce the efficiency of chitosan uptake due to the participation of amino groups in the crosslinking procedure. Therefore, the interpolation of special functional crosslinking agents known for their high performance such as ethylene-di amine tetra acetic acid (EDTA) (22), and ionic surfactants like cetyltrimethyl-ammonium bromide (CTAB) and sodium dodecyl sulfate (SDS) (23, 24) is an influential modification method to reinforce their adsorption capacity and selectivity. Accordingly, we have recently reported a new simple approach for fabrication of some nanocomposites such as cross-linked chitosan/glauconite clay, EDTA-chitosan modified glauconite, CTAB-modified chitosan/glauconite, and SDS-modified chitosan/glauconite composites. These prepared nanocomposites showed high efficiency in removing fluoride ions from wastewater. On the other hand, due to the high toxicity of Mn(II) ions at higher concentrations and the various functional groups that the as-prepared nanocomposites have, we herein report on the removal of Mn(II) ions from polluted water utilizing the aforementioned nanocomposites. Various influencing factors on the adsorption process have been examined such as initial pH, contact time, dosage, etc. The experimental data were examined using different isotherm models. The kinetics and thermodynamics of the adsorption process were also estimated. Also, regeneration of the prepared adsorbents was investigated in this study.

2. Experimental

2.1 Materials and reagents

Raw Glauconite clay (G) with chemical content of SiO_2: 50.50 %, Fe_2O_3: 20.88%, Al_2O_3: 7.88 %, K_2O: 5.00%, MgO: 2.81%, CaO: 0.34%, SO_3: 1.2% and Na_2O: 0.95% was collected from El-Gideda area, Egypt. Chitosan (CS) (Deacetylation degree >85%), cetyltrimethyl ammonium bromide (CTAB), and sodium dodecyl sulfate (SDS) were purchased from Sigma Chemical Co., USA. All other chemicals were of analytical grade e.g. acetic acid; sodium hydroxide, HCl, and glutaraldehyde (GL) also were used without further purification as received from El-Nasr Pharmaceutical Chemicals Company (ADWIC)-Company, Egypt. The standard solutions of manganese ion was prepared by dilutions of stock solution (1000 mgL^{-1}), which were purchased from Merck. pH value of the adsorption media was adjusted when required using 0.2 N HCl and/or NaOH solutions. De-ionized water was used for all preparations.

2.2. Adsorbent preparation

The preparation methods of glauconite clay (G), cross-linked chitosan/glauconite clay (GL-CS/G) composite, EDTA-chitosan modified glauconite (EDTA-GL-CS/G) composite, and surfactant-modified chitosan/glauconite (CTAB-CS/G and SDS-CS/G) composite preparation were reported by our research group elsewhere (25).

2.3. Materials characterization

The chemical and mineralogical characterization of the raw glauconite and the as-prepared composites were reported earlier (25). The manganese ion concentration was determined by atomic absorption spectrophotometer (Unicam, Solar 929, UK supplied with acetylene and nitrous oxide burner heads) at 279.5 nm resonance line according to the reported standard method (26). The pH value was measured using pH-meter model Sension 3 (Huch, USA). The zero point charge of the adsorbents (pHzpc) was estimated by the pH drift method (27) using 0.01 M NaCl solutions at different pH values varied between 2 to 10.

2.4. Adsorption studies

The application of raw glauconite clay and its as-prepared composites as adsorbents for manganese ion removal was explored using batch technique. To study the equilibrium system of adsorption, adsorbent weight of 0.1 g was taken into intimate contact with manganese solutions (0.05 L) of different concentrations ranging from 10 to 300 mgL^{-1}. The admixtures were magnetically stirred (350 rpm stirring speed) at a temperature of 25 ºC, specific pH value adjusted using 0.2N NaOH or 0.2N HCl solutions and a predetermined time intervals. Then, the adsorbents were filtered and the residual manganese concentration in the filtrate was analyzed by atomic absorption spectrophotometer using a pre-constructed calibration curve for the manganese cation.

The removal efficiency percent (%R), capacity (q_t, mgg^{-1}), and the equilibrium capacity (q_e, mgg^{-1}) of the adsorbent were estimated using equations (1), (2), and (3), respectively.

$$\%R=[(C_0-C_t)/C_0]\times100 \quad (1)$$

$$q_t=V(C_0-C_t)/m \quad (2)$$

$$q_e=V(C_0-C_e)/m \quad (3)$$

Where C_0 (mgL^{-1}) is the initial manganese concentration, C_t (mgL^{-1}) is the remaining manganese concentration, and C_e (mgL^{-1}) is the equilibrium manganese concentration at time 0, t, and equilibrium time, respectively, for the adsorption. While m(g), and V(L) are the weight and the volume of adsorbent and solution, respectively.

3. Results and discussion

In our earlier studies, we reported on the preparation of glauconite clay (G), cross-linked chitosan/glauconite clay (GL-CS/G), EDTA-chitosan modified glauconite (EDTA-GL-CS/G), and surfactant-modified chitosan/glauconite (CTAB-CS/G and SDS-CS/G) composites (2). We also

reported previously on the characterization of these materials using different techniques including Fourier-transform infrared spectroscopy (FTIR), X-ray diffraction (XRD), field emission scanning electron microscopy (FE-SEM), nitrogen physical adsorption (BET), atomic absorption spectrophotometry (AA), and thermal gravimetric analysis (TGA). Additionally, these nanocomposites were used in that previous work for the removal of fluoride ions from aqueous solutions. In the present study, as a continuation to our research, we have applied the aforementioned nanocomposites as adsorbents for the removal of manganese(II) ions from aqueous media due to its high toxicity at higher concentrations than the permissible limits (8). However, the point of zero charge (pHpzc) values of these adsorbents have not been reported previously. Due to their importance, we have started our current research by their estimation as will be shortly mentioned.

3.1. Determination of point of zero charge (pH_{pzc}) values of the glauconite nanocomposite adsorbents

The point of zero charge (pH_{pzc}) value of the adsorbent is essential for a better understanding the adsorption mechanisms; it is well-defined as the pH value where the adsorbent surface has no charge in specific adsorption. At a pH higher than pH_{pzc}; the surface of adsorbents carries a negative charge and thus favors absorption of cations. At a pH lower than pH_{pzc}; the adsorbent carries a positive charge and thus prefers the adsorption of anions (22). Values of pH_{pzc} were determined by the pH drift method. In this method, adsorbent suspensions in 0.01 M NaCl solutions with different initial pH values (2-10) were used for this assessment. The final pH (pH_{final}) values were then plotted against the initial pH ($pH_{initial}$) values for each adsorbent, Fig. 1, and from these figures the pH_{pzc} values were determined. The pH_{pzc} values of G, GL-CS/G, EDTA-

GL-CS/G, SDS-CS/G, and CTAB-CS/G products were found to be 6.40, 5.72, 5.88, 5.78, and 5.61, respectively. Variation in pH_{pzc} of adsorbents in this study may be due to the structural changes during the modification process. These results indicate that the performed G clay modification has a significant effect on its particle charges which may in turn has a positive impact on the adsorption efficiency toward the manganese cations.

< Fig. (1)>

3.2. Adsorption studies

Adsorption properties of G, GL-CS/G, EDTA-GL-CS/G, SDS-CS/G and CTAB-CS/G adsorbents were explored using Mn(II) ions as an adsorbate model. Therefore, several parameters influencing the adsorption process such as pH, contact time, adsorbent dosage, initial Mn(II) ion concentration, and temperature were studied.

3. 2.1. Effect of pH

The influence of pH on the Mn(II) ion adsorption using G, GL-CS/G, EDTA-GL-CS/G, SDS-CS/G, and CTAB-CS/G adsorbents was examined in the pH range of 2-7. For this experiment the adsorption working conditions were: 50 mgL^{-1} initial Mn(II) ion concentration (C_0), 1g for G adsorbent and 0.1 g for GL-CS/G, EDTA-GL-CS/G, SDS-CS/G, and CTAB-CS/G adsorbents, separately, 24 h contact time, and 25 ^oC temperature. The results as displayed in Fig. 2 revealed that the adsorption amount of Mn(II) ion increased with increasing the initial pH value until it reached equilibrium at pH 6.5. Afterward, the precipitation of metal ion hydroxides takes place.

This behavior can be interpreted on the basis of the point of zero charge. Consequently, at acidic pH values (i.e. pH<6.4), the Mn(II) ion adsorption was low due to the competition between two positively charged H^+ and Mn(II) ions for the adsorption sites, and thus, the net interaction is an electrostatic repulsion, which resulting in reduction of Mn(II) ion adsorption (28). With a gradual rise in pH value until 6.5, linked H^+ is released from the active sites leaving more vacant sites for more Mn(II) ion adsorption. Beside, this pH value extent is close to the pH_{pzc} at which the surface of clay is surrounded by OH^- ions and become negatively charged which in turn attract more positively charged Mn(II) ion due to the electrostatic attraction (29). With increasing the pH value toward more basic pH condition, these active sites are gradually de-protonated and the Mn(II) ion was hydrolyzed resulting in formation and precipitation of a large number of hydroxides such as $Mn(OH)^+$, $Mn_2(OH)_3$, $Mn(OH)_2$, $Mn_2(OH)^+_3$ and $Mn(OH)_4^{2-}$ species (30, 31).

On the other hand, the chitosan amino groups in the GL-CS/G, EDTA-GL-CS/G, SDS-CS/G and CTAB-CS/G composites were protonated at lower pH value and appeared in the form of $-NH^{3+}$ which in turn increasing the electrostatic repulsion with Mn(II) ions and resulting in a decline in Mn(II) ions adsorption. On contrary, with a gradual increase in pH value, the amino groups are deprotonated and abundant OH^- ions created a competitive environment for the adsorption surface sites due to the elctrostatic attraction between positive charged Mn(II) ion and adsorbents surface sites with negative charge; thus, the increases in removal percent were observed. At a higher pH value above 6.5, the cumulative effect of Mn(II) ions adsorption as well as precipitation may be happened. Depending on the above mentioned results, the pH of 6.50 was selected as the optimum pH value for further adsorption experiments to avoid the interference of results associated with the precipitation of metal ions at higher pH value.

<Fig. 2>

3.2.2. Effect of adsorbent dosage

The adsorbent dosage is one of the most important factors that affecting the metal ions adsorption due to its effect on the number of binding sites and the total surface area of adsorbent. The effect of adsorbent dosage on the Mn(II) ions removal was studied under the prior operating conditions except the amount of adsorbent. As depicted in Fig. 3(a,b) the removal performance of Mn(II) ions was firstly enhanced until a specific dose of adsorbent, and then reduced as the amount of adsorbent increased. This trend can be attributed to the increase in the adsorptive active sites on the adsorbent surface with the increase in the adsorbent dose up to agiven dose (32), and then the aggregation of the nanoparticles is occurred. This aggregation brought about a reduction in the total available adsorbent surface sites for Mn(II) ion adsorption, which led to a decrease in the adsorption performance of the adsorbent. These results are consistent with the published data for the adsorption of orange G textile dye on some nano-adsorbents (33). According to the obtained results, 1g of G and 0.15 g of GL-CS/G, EDTA-GL-CS/G, SDS-CS/G, and CTAB-CS/G adsorbents were selected as the optimum adsorbent amounts for subsequent studies. The results also exhibited that the adsorption increased in the order of SDS-CS/G > EDTA-GL-CS/G > CTAB-CS/G > GL-CS/G > G. The high removal performance of Mn(II) ions on SDS-CS/G adsorbent can be ascribed to the interlayer spacing produced from intercalation of G clay with chitosan polymer as well as the presence of anionic SDS surfactant that changing the G surface from hydrophobic to hydrophilic resulting in a high adsorption of Mn(II) ion onto both inner and outer adsorbent surface.

<Fig. 3(a,b)>

3.2.3. Effect of contact time

Effect of adsorption time on Mn(II) ions removal was investigated over different time intervals (0-300 min) under working conditions: 0.05 L of Mn(II) ions solution with 50 mgL^{-1} initial concentration, 25 ^{o}C temperature, pH6.5, 1g of G and 0.15 g of GL-CS/G, EDTA-GL-CS/G, SDS-CS/G and CTAB-CS/G adsorbents. Fig. 4(a,b) illustrated that the removal of Mn(II) ions was improved by increasing the contact time. The percentage of Mn(II) ions uptake using the G adsorbent was initially fast, and then gradually slowed down until reached saturation after 60 minutes. Hence, for further experiments, 60 minutes was fixed as an optimum contact time for the G adsorbent. On the other hand, GL-CS/G, EDTA-GL-CS/G, SDS-CS/G and CTAB-CS/G composites showed higher adsorption capacities and reached equilibrium after 240 minutes. This contact time was also fixed as the optimum contact time for further experiments, for these composite adsorbents. During the initial stage of adsorption, the rapid uptake is probably due to the availability of the large number of vacant active sites on the adsorbents surface. However, the slow uptake in the later stages are probably generated by less available adsorption active sites, followed by Mn(II) ions saturation on the surface of adsorbents (34).

<Fig. 4.>

3.2.4. Effect of initial metal ion concentration

The effect of initial concentration of the Mn(II) ions on the aforementioned adsorbents efficiency was examined at different initial Mn(II) concentrations in the range of 10-300 mg/L at pH 6.5, 25 ºC, using 1g of G and 0.15 g of GL-CS/G, EDTA-GL-CS/G, SDS-CS/G and CTAB-CS/G adsorbents. Fig. 5(a,b) demonstrates that by increasing the initial Mn (II) concentration, the equilibrium adsorption capacity of Mn(II) was enhanced up to an initial concentration of 200 mg/L after which a plateau behavior was attained. This behavior can be explained on the basis that increasing the initial Mn(II) concentration leads to an increased availability of a greater number of Mn(II) ions at the solid–solution interface, which in turn brings about a higher concentration gradient. Whereas, the constant adsorption capacity observed at an initial metal concentration exceeding 200 mgg^{-1} indicates that all surface active sites having a higher affinity towards Mn(II) ions were saturated. These results are consistent with the published data for the adsorption of manganese on kaolinite clay particles (35).

<Fig. 5.>

3.3. Adsorption kinetics

To explore the adsorption mechanism and the efficacy of the adsorption process, some kinetic models such aspseudo-first-order, pseudo-second-order, and intra-particle diffusion models. Pseudo-first-order (Eqn. 4) and pseudo-second-order (Eqn. 5) kinetic models are expressed according to the following equations (36-38):

$$\log(q_e - q_t) = \log q_e - \frac{k_1}{2.303}\, t \qquad (4)$$

$$\frac{t}{q_t} = \frac{1}{k_2 q_e^2} + \frac{1}{q_e}\, t \qquad (5)$$

Where, q_t and q_e (mgg^{-1}) are the amounts of metal ions adsorbed at time t (min) and at equilibrium, respectively. k_1 (min^{-1}) is the first-order rate constant. Values of q_e and k_1 constants

were determined from the intercept and slope of the plot of $\log(q_e - q_t)$ versus t (results not shown). The kinetic parameters; k_1 and correlation coefficients (r^2), were listed in Table 1. Additionally, values of k_2 and q_e constants of the pseudo-second-order model can be estimated from the intercept and slope of the linear plot of t/q_t versus t (Fig. 6(a)). The parameters; correlation coefficients (r^2) and k_2, of the pseudo-second-order model were tabulated in Table 1. By comparison between experimental and calculated pseudo-first-order and pseudo-second-order model values, the results exhibited good fitness of the pseudo-second-order model for the adsorption process of Mn(II) ions. This is due to that the experimentally obtained $q_{e(exp)}$ values from this model are more compatible with the calculated $q_{e(cal)}$ ones. Besides, the r^2 values from this model were closer to 1.

The data of adsorption was also analyzed using the Weber's intra-particle diffusion model to elucidate the diffusion mechanism. The intra-particle diffusion model (Eqn. (6)) is given as (39):

$$q_t = k_{id} t^{0.5} + c \qquad (6)$$

Where k_{id} ($(mgg^{-1})\ min^{-1/2}$) is rate constant and C (mgg^{-1}) is the intercept. The larger intercept value, the larger is the surface adsorption contribution in the rate-controlling step. k_{id} constant is obtained from the slope of q_t versus $t^{1/2}$ plot. As displayed in Fig. 6(b), the linear part along the curves of q_t versus $t^{1/2}$ did not pass through the origin and all of them are multi-linear plots. Therefore, it was concluded that the of Mn(II) ions adsorption on the G clay and the as-prepared composites was complex and controlled not only by the intra-particle diffusion mechanism, but also by various mechanisms such as bulk diffusion and film diffusion mechanisms (40).

<Fig. 6.>

<Table 1>

3.4. Adsorption isotherm studies

To verify how the metal ions are partitioned between the adsorbents and liquid phases at equilibrium, the adsorption results were examined using some isotherm models such as Langmuir, Freundlich, and Dubinin-Radushkevich models. The linear forms of Langmuir and Freundlich isotherm equations can be expressed as in Eqns. (7) and (8), respectively (41, 42).

$$\frac{C_e}{q_e} = \frac{1}{q_m b} + \frac{C_e}{q_m} \quad (7)$$

$$\ln q_e = \ln K_F + \frac{1}{n} \ln C_e \quad (8)$$

Where q_e is the monolayer adsorption capacity of the adsorbent (mgg^{-1}), q_m is the maximum adsorption capacity (mgg^{-1}), and b is Langmuir constant (Lmg^{-1}) which reflects the affinity between the adsorbate and the adsorbent. K_F ((mgg^{-1}) (Lmg^{-1})$^{1/n}$) and n are Freundlich constants which related to the adsorption capacity and intensity of the adsorbents, respectively. Langmuir isotherm supposes a monolayer adsorption on homogenous surfaces without interactions between the adsorbed molecules whereas; Freundlich isotherm presumes a multilayer adsorption of the adsorbate species on heterogeneous surfaces. According to Langmuir isotherm, q_m and b values were computed from the linear regression analysis of C_e/q_e vs C_e plot as represented in Fig. 7(a). Additionally, depending on the Freundlich adsorption isotherm, the Freundlich constants (n and K_F) are determined from the intercept and slope of $\ln q_e$ vs $\ln C_e$ plot as represented in (Fig. 7(b)). The Langmuir and Freundlich isotherm constants are listed in Table (2). Furthermore, q_m can be computed from the Freundlich isotherm model according to Eqn. (9) (43):

$$K_F = q_m/C_0^{(1/n)} \quad (9)$$

Obviously, from the data listed in Table (2), the adsorption process can be described well using Langmuir isotherm model compared to the Freundlich isotherm model. This is based on the higher correlation coefficient (R^2) values and the high compatibility between the calculated q_m ($q_{m(cal)}$) and the experimental q_m ($q_{m(exp)}$) values. The q_{max} values obtained from Langmuir model were found to be in the order of SDS-CS/G > EDTA-GL-CS/G > CTAB-CS/G > GL-CS/G > G. This trend can be ascribed to the following reasons. (1) The presence of negatively charged surface of the G clay with a huge number of exchangeable ions can result in coating its surface with a water molecule layer; therefore, it showed strong hydrophilicity and high adsorption capacity towards Mn(II) ions. (2) Addition of large amounts of –OH and $–NH_2$ functional groups, due to the combination of G and chitosan polymer, can result in enhancement in the adsorption capacity towards Mn(II) ions. (3) Further addition of functional groups such as carboxylic groups (–COOH) in EDTA-GL-CS/G composite can bring about increasing the negative charge surface which in turn resulting in more electrostatic attraction of Mn(II) ions (44). (4) Furthermore, functionalization of the composite with organic anions such as anionic surfactants (SDS) can show more enhancements in their adsorption capacity towards Mn(II) ions. Besides, the negatively charged hydrophilic heads (sulfonate groups ($-OSO_3-$)) of the anionic SDS surfactant might increase the negative surface potentially when they pointed towards the bulk of the solution; and consequently resulting in a strong electrostatic attraction of Mn(II) ions. Hence, the removal would be enhanced. However, with the reference to CTAB-CS/G adsorbent, its adsorption capacity was noticeable although it includes hydrophobic head with a positive charge surface. This is probably returning to electrostatic interaction between the functional groups of the chitosan itself and the ordinary adsorption of the ions inside the pores of the G clay as well (45).

In addition, the essential features of the Langmuir isotherm can be demonstrated regarding to dimensionless separation factor constant (R_L) as follows:

$$R_L = \frac{1}{1+bC_0} \qquad (10)$$

Where C_0 (mg/L) and b (L/mg) are the initial metal ion concentration and the Langmuir equilibrium constant, respectively. The separation factor values afford essential information about the adsorption process nature, which it may be linear (R_L= 1), irreversible (R_L= 0), favorable (0 < R_L< 1) or unfavorable (R_L> 1) (46). R_L values were estimated at different initial concentrations ranged from 10 to 300 mg L^{-1} and tabulated in Table 3. For all the experimental data, values of R_L were found to be lying between 0 and 1, indicating favorable adsorption of Mn(II) ions on all adsorbents at all concentrations. Further, the adsorption of Mn(II) ions was considered as favorable because the Freundlich exponent (n) values were found to be >1 and in the range of 3.27-5.18 (47).

<Fig. 7.>

<Table 3.>

Furthermore, the equilibrium data was examined using Dubinin-Radushkevich isotherm model (D-R model). The linearity of D-R model (Eqn. (11)) can be defined as (48):

$$\ln q_e = \ln q_m - \beta\varepsilon^2 \qquad (11)$$

Where q_e and q_m (mg/g) are the equilibrium and the maximum adsorption capacity of the adsorbent, respectively. ε (Polanyi potential) = RT ln(1+(1/C_e), R (8.314 J mol^{-1} K^{-1}) is the universal gas constant and T (K) is the absolute temperature. β (mol^2/kJ^2)) is the Dubinin-

Radushkevich constant associated with the adsorption energy. The D–R constants q_m and β values can be detected from the slope and intercept of the plot of $\ln q_e$ against ε^2 as presented in Fig. 7(c). The adsorption energy (E) can be determined from the following equation (Eqn. (12)).

$$E = \sqrt{\frac{1}{2\beta}} \qquad (12)$$

Notably, the E values obtained from the present study were found to be < 8 kJ mol^{-1} as presented in Table 3, indicating the physisorption of Mn(II) ions on the adsorbents under investigation because the values are in the range of 5–40 kJ mol^{-1} declared for the physisorption (49). However, the results did not follow well the D-R model, based on the obtained lower correlation coefficient (r^2) values. According to the above discussion, it could be concluded that Mn(II) ions adsorption on the aforementioned adsorbents was a monolayer coverage since the estimated experimental data complied well with the Langmuir isotherm model compared to other applied isothermal models where, the estimated q_m values were closer to the $q_{m(exp)}$ values and the r^2 values were closer to unity.

<Table.3>

3.5. Thermodynamic study

Thermodynamics parameters associated with the adsorption process such as Gibbs free energy change (ΔG°), entropy change (ΔS°), and enthalpy change (ΔH°) were examined to check the influence of temperature on Mn(II) ion adsorption under different temperature values (298-318 K) by applying Eqns (13) and (14) (50, 51).

$$\ln K_c = \Delta S°/R - \Delta H°/RT \qquad (13)$$

$$\Delta G° = \Delta H° - T\Delta S° \qquad (14)$$

Where K_c is a thermodynamic equilibrium constant. T and R are absolute temperature (K) and universal gas constant (8.314 $J \cdot mol^{-1} \cdot K^{-1}$), respectively. Regarding to Eqn. (15), K_c is a constant with a dimensionless unit (51-53).

$$\Delta G^o = -RT\ln K_c \qquad (15)$$

Hence, the dimensionless thermodynamic equilibrium constant (K_c) was examined using the distribution coefficient constant (K_d) approach (52). In this respect, the distribution coefficient constant ($K_d=q_e/C_e$) was first estimated by graphing $\ln(q_e/C_e)$ against q_e and extrapolating q_e to zero. Then K_d was corrected owing to the method proposed by Milonjić to derive the thermodynamic equilibrium constant K_c ($K_c = K_d \times 1000$) (53). According Eqns. (13-14), ln K_c vs. 1/T was plotted (Fig. 8) and from the intercept and slope the ΔH^o and ΔS^o values were calculated, then ΔG^o values were estimated. The thermodynamic constants were tabulated in Table (4). The ΔG^o values were found to be in the ranges of (-14.5 to -15.8), (-15.50 to -16.60), (-17.10to -18.60), (-17.50 to -18.80), and (-16.0 to -17.2 $kJmol^{-1}$) for G, GL-CS/G, EDTA-GL-CS/G, SDS-CS/G and CTAB-CS/G adsorbents, respectively. Moreover, the results also indicated the spontaneous nature of Mn(II) ions sorption on the aforementioned adsorbents because it was found that the values of ΔG^o increase in the negative direction with increasing the temperature. Additionally, the positive enthalpy (ΔH^o) indicates the endothermic nature of the adsorption process. The positive ΔS^o values for all aforementioned adsorbents revealed an increase in the randomness at the solid-solution interface during the adsorption process which in turn indicated an accumulation of Mn(II) ions (54). In general, based on the calculated $\Delta H°$ and ΔG^o values, it can be concluded that the adsorption of Mn(II) ions on the aforementioned adsorbents is a physisorption as ΔH^o values is smaller than 40 kJ mol^{-1}, and $\Delta G°$ values lies in the range of -20 to 0 kJ mol^{-1} which is characteristic to the physisorption process (55).

<Fig. 8>

<Table 4.>

3.6. Mechanism of Mn(II) ions adsorption on the G clay and its nanocomposites

The current study revealed that the mechanism of Mn(II) ions adsorption not only depends on the number of functional sites in the applied adsorbent but also on the changing in the pH value as illustrated in Scheme (1). The removal of Mn(II) ions was small at low pH values (pH < 5) then it increased slowly until it reached maximum at higher pH values (ca. pH 6.5). Based on the results, the mechanism of the manganese ion removal depended on the pH value and the structure of the utilized adsorbents. There are various adsorption/exchange sites present in the G clay since it contains various hydrous oxides such as SiO_2, Fe_2O_3, Al_2O_3, and others (56). Accordingly, the adsorption mechanisms of Mn^{2+} ions on G clay and its nanocomposites are summarized in Scheme 1. Where, -G represents the intrinsic sites the glauconite clay. The glauconite clay has on its surface hydroxyl functional groups (-GOH) at which adsorption of the contaminants is frequently occurring. The surface hydroxyl groups are amphoteric; therefore, they are turned into positively charged hydroxylated sites (GOH_2^+) at pH values lower than the pH_{pzc} values of the prepared compounds (Eqn 1, Scheme 1). The amino groups of the modified chitosan nanocomposites are also protonated in the acidic media, according to Eqns 2 and 3 (Scheme 1), and converted into positively charged functional groups. Similar results are published for other chitosan composites (57). Consequently, in acidic media, the adsorption efficiency will be low due to the electrostatic

463 repulsion between the Mn^{2+} ions and the aforementioned positively charged functional groups.
464 The removal of Mn^{2+} ions can also proceed by the ion exchange mechanism, according to Eqn 4
465 (Scheme 1). As such, every one Mn^{2+} ion can exchange two K^{+} cations of that clay. Furthermore,
466 the removal of Mn^{2+} ions by utilizing the chitosan composites is probably due to some adsorption
467 processes through the porous structure of the G clay and some complexation interactions between
468 the manganese ions and oxygen and/or nitrogen atoms of functional groups of those composites
469 as well, as presented in Eqns (5) and (6) in Scheme 1. These results are compatible with some
470 reported mechanisms (56, 58). On the contrary, the removal efficiency enhanced by increasing the
471 pH value above pH_{pzc} values of the G clay (pH_{pzc} = 6.4) and its nanocomposites (pH_{pzc}= 5.61-5.88).
472 This is attributing to the electrostatic attraction between Mn^{2+} cations and the negatively charged
473 particles of G clay and its nanocomposites at those higher pH values (Eqns 5 and 7; Scheme 1).
474 Where, at those pH values, the hydroxylated sites of the G clay, amino groups of the chitosan
475 composites, and carboxylic groups of the EDTA modified composites may undergo deprotonation,
476 as outlined in Eqns (7), (9), and (11). This resulted in an enhancement of the electrostatic attraction
477 and/or complexation between Mn^{2+} cations and the negatively charged groups such as $–GO^{-}$, $–NH^{-}$
478 and $–COO^{-}$ of the G clay, chitosan, and EDTA components of the nanocomposites, respectively,
479 as presented in Eqns (8), (10), and (12). These adsorption mechanisms are compatible with the
480 reported ones for similar EDTA-modified molecules (59). The CTAB component of the CTAB
481 modified nanocomposite may also played a role in the manganese removal in addition to the
482 aforementioned significant roles. The contribution of CTAB in the removal process is probably
483 through a weak complexation between the manganese cations and the nitrogen atoms of its tertiary
484 amino groups ($(CH_3)_3N$-) and its bromide ions in the presence of some hydroxide anions, at
485 alkaline pH values (Eqn 16, Scheme 1). The suggested mechanism for the adsorption by using

CTAB-modified composite is in accordance with those reported for similar composites modified with some cationic surfactants (60). It is worth noting that the SDS-CS/G composite brought about the highest manganese removal percentage. This is probably attributing to the contribution of the sulfonate headgroups of the SDS surfactant in the adsorption process for this composite, as represented in Eqns 13 and 14 in Scheme 1, along with the aforementioned roles of the G clay and chitosan components of this composite. Where, the sulfonate groups ($-OSO_3-$) may undergo ionization at higher pH values (Eqn 13 in Scheme 1). Then, there will be an electrostatic attraction and/or complexation between these negatively charged sulfonate groups and Mn^{2+} cations, which resulted in the highest removal efficiency compared to the other studied adsorbents. Besides, the removal by using the SDS-CS/G nanocomposite may also proceed through an additional cation exchange mechanism between Na^+ ions of the SDS component and Mn^{2+} ions in the solution (Eqn. 15; Scheme 1). The suggested mechanism for SDS-modified nanocomposite is consistent with those reported for similar modified anionic surfactant composites (61). Additionally, it is reported that generally the adsorption of metal ions can include surface precipitation, physical and chemical adsorption, and ion exchange (56). Similar behavior has been reported for adsorption of Cu ions (62).

<Scheme 1>

3.7. Regeneration studies

Regeneration and reuse of any used adsorbent is an important factor to make the sorption process economic. Therefore, we studied the reusability and regeneration of the used raw gluconite clay and its as-prepared nanocomposites. The adsorption of Mn(II) ions was achieved under optimal adsorption conditions for 4 h contact time, pH 6.5 at room temperature ca. 25 $^{\circ}$C±1.

Subsequently, the loaded adsorbents were recovered in 1M HCl as an eluent, then washed with distilled water, and finally drying in oven at 60 ºC. The regenerated adsorbents were reused for Mn(II) ions adsorption and the spent adsorbents were recovered again and subjected to another adsorption cycle. All adsorbents were reused for 4 times after their first regeneration. The results were illustrated in Fig.9. The maximum adsorption capacities (q_m) for the sorption/desorption cycles were found to be 3.59, 3.40, 3.1 and 2.65 $mgg^{-1}$for G; 23.90, 23.01, 22.54 and 21.11 $mgg^{-1}$for GL-CS/G; 25.78, 25.60, 24.78 and 23.01 $mgg^{-1}$for EDTA-GL-CS/G; 26.12, 26.00, 25.76 and 24.11$mgg^{-1}$for SDS-CS/G; and 25.47, 25.32, 24.31 and 22.66mg/g for CTAB-CS/G. The results obtained indicated that the prepared adsorbents had excellent regeneration ability and good performance for the frequent use up to at least four cycles. These results also confirmed that gluconite clay and its modified forms could be regenerated and reused to treat wastewater contaminated with Mn(II) ions.

<Fig. 9>

3.8. Comparison with other adsorbents

Finally, a comparative evaluation of q_m (maximum adsorption capacity) of the Mn(II) ions adsorption on the aforementioned adsorbents in the current study with those previously reported data. According to Table 5, the as-prepared G nanocomposites have relatively higher q_m values compared to most of the tabulated adsorbents for Mn(II) ions removal. Despite, the adsorption capacity of G was relatively low compared to that of the as-prepared nanocomposites in the current study; it was higher than well-known adsorbents such as activated kaolinites, activated carbon, and zeolite. This indicates that the modified G clay nanocomposites are

promising and relevant candidates as well as have long-term applicability for the removal of Mn(II) ions from aqueous media.

<Table 5 >

3.9. Application to real wastewater samples

To highlight the performance of the examined adsorbents to remove Mn(II) ions and how they are applied to the wastewater, water samples were collected from wastewater pools before being treated at the treatment unit at Abu Zaabal for Fertilizers and Chemicals Company (AZFC), Egypt. The chemical composition of the collected water samples as well as the batch adsorption conditions of the experiments were conducted according to the Standard Methods for the Examination of Water and Wastewater (63) as reported previously (25). The chemical composition of wastewater was analyzed and summarized in Table (6). The concentration of Mn(II) ions in the filtrate was estimated using an atomic absorption spectrophotometer. It is noteworthy that the adsorption experiments were conducted as reported before at pH 6. Results expressed that the maximum adsorption rate of Mn(II) ions removal on the G, GL-CS/G, EDTA-GL-CS/G, SDS-CS/G, and CTAB-CS/G adsorbents were determined to be 94.10%, 81.85%, 83.90%, 86.18% and 82.42%, respectively. Indicating high efficiency and chemical stability of the aforementioned adsorbents for removing the Mn(II) ions from wastewater even though the presence of foreign ions (cations and anions), which can well interfere and compete through the adsorption process.

Conclusions

In summary, this study explored the Mn(II) ions adsorption from polluted aqueous solutions onto raw gluconite clay and its prepared modified chitosan nanocomposites. The used

chitosan was modified with glutaraldehyde (GL), ethylenediaminetetraacetic acid (EDTA), sodium dodecyl sulfate (SDS) and cetyltrimethyl ammonium bromide (CTAB), for producing nanocomposites: GL-CS/G, EDTA-GL-CS/G, SDS-CS/G, and CTAB-CS/G, respectively. Various experimental conditions influencing the adsorption process such as pH, adsorbent amount, and contact time were examined. The adsorption results showed that SDS-CS/G nanocomposite has the highest adsorption capacity (27.74 mgg^{-1}) toward the removal of Mn(II) ions from polluted aqueous media. Moreover, the Langmuir isotherm and the pseudo-second-order kinetic model fitted well the adsorption process. The positive $\Delta H°$ values and the negative $\Delta G°$ values demonstrated that the process of Mn(II) ions adsorption was endothermic and spontaneous. Eventually, overall these aspects, including high adsorbents capacity, low cost and the possibility of regeneration make the as-prepared nanocomposites as a promising candidate adsorbents for removing Mn(II) ions from polluted aqueous solutions.

Acknowledgments

The authors are thankful to the unidentified reviewers whose comments and recommendations have significantly improved the quality of this manuscript.

References

1. Yang J, Huang B, Lin M. Adsorption of Hexavalent Chromium from Aqueous Solution by a Chitosan/Bentonite Composite: Isotherm, Kinetics, and Thermodynamics Studies. Journal of Chemical & Engineering Data. 2020;65(5):2751-63.

2. Sobeih MM, El-Shahat MF, Osman A, Zaid MA, Nassar MY. Glauconite clay-functionalized chitosan nanocomposites for efficient adsorptive removal of fluoride ions from polluted aqueous solutions. RSC Advances. 2020;10(43):25567-85.

3. Alvarez-Bastida C, Martínez-Miranda V, Solache-Ríos M, Linares-Hernández I, Teutli-Sequeira A, Vázquez-Mejía G. Drinking water characterization and removal of manganese. Removal of manganese from water. Journal of Environmental Chemical Engineering. 2018;6(2):2119-25.

4. Mehrali-Afjani M, Nezamzadeh-Ejhieh A. Efficient solid amino acid–clinoptilolite nanoparticles adsorbent for Mn(II) removal: A comprehensive study on designing the experiments, thermodynamic and kinetic aspects. Solid State Sciences. 2020;101:106124.

5. Nadaska G, Lesny J, Michalik I. Environmental aspect of manganese chemistry. 2012. Hungarian Electronic Journal of Sciences–http://heja szif hu/ENV/ENV-100702-A/env100702a pdf Cited. 2018;17.

6. Yadav VB, Gadi R, Kalra S. Clay based nanocomposites for removal of heavy metals from water: a review. Journal of environmental management. 2019;232:803-17.

7. Basu N, Nam D-H, Kwansaa-Ansah E, Renne EP, Nriagu JO. Multiple metals exposure in a small-scale artisanal gold mining community. Environmental research. 2011;111(3):463-7.

8. Li Y, Xu Z, Ma H, S Hursthouse A. Removal of Manganese (II) from Acid Mine Wastewater: A Review of the Challenges and Opportunities with Special Emphasis on Mn-Oxidizing Bacteria and Microalgae. Water. 2019;11(12):2493.

9. Carolin CF, Kumar PS, Saravanan A, Joshiba GJ, Naushad M. Efficient techniques for the removal of toxic heavy metals from aquatic environment: A review. Journal of environmental chemical engineering. 2017;5(3):2782-99.

10. Nassar MY, Ahmed IS, Hendy HS. A facile one-pot hydrothermal synthesis of hematite (α-Fe2O3) nanostructures and cephalexin antibiotic sorptive removal from polluted aqueous media. Journal of Molecular Liquids. 2018;271:844-56.

11. Nassar MY, Ali EI, Zakaria ES. Tunable auto-combustion preparation of TiO2 nanostructures as efficient adsorbents for the removal of an anionic textile dye. RSC Advances. 2017;7(13):8034-50.

12. Wingenfelder U, Nowack B, Furrer G, Schulin R. Adsorption of Pb and Cd by amine-modified zeolite. Water Research. 2005;39(14):3287-97.

13. Djomgoue P, Siewe M, Djoufac E, Kenfack P, Njopwouo D. Surface modification of Cameroonian magnetite rich clay with Eriochrome Black T. Application for adsorption of nickel in aqueous solution. Applied surface science. 2012;258(19):7470-9.

14. Wu Q, Xue Z, Qi Z, Wang F. Synthesis and characterization of PAn/clay nanocomposite with extended chain conformation of polyaniline. Polymer. 2000;41(6):2029-32.

15. Koksal E, Afsin B, Tabak A, Caglar B. Structural characterization of aniline-bentonite composite by FTIR, DTA/TG, and PXRD analyses and BET measurement. Spectroscopy Letters. 2011;44(2):77-82.

16. Yatsyshyn M, Saldan I, Milanese C, Makogon V, Zeffiro A, Bellani V, et al. Properties of glauconite/polyaniline composite prepared in aqueous solution of citric acid. Journal of Polymers and the Environment. 2016;24(3):196-205.

17. Elsergany M, Shanableh A, Ahsan A. EXPLORATORY STUDY TO ASSESS THE IMPACT OF CHITOSAN/BENTONITE RATIO ON THE METAL REMOVAL CAPACITY OF CHITOSAN MODIFIED BENTONITE CLAY. GLOBAL NEST JOURNAL. 2016;18(2):437-43.

18. Pardo L, Domínguez-Maqueda M, Cecilia JA, Pozo Rodríguez M, Osajima J, Moriñigo MÁ, et al. Adsorption of Salmonella in Clay Minerals and Clay-Based Materials. Minerals. 2020;10(2):130.

19. Vanamudan A, Bandwala K, Pamidimukkala P. Adsorption property of Rhodamine 6G onto chitosan-g-(N-vinyl pyrrolidone)/montmorillonite composite. International journal of biological macromolecules. 2014;69:506-13.

20. Zhou Y, Gao B, Zimmerman AR, Fang J, Sun Y, Cao X. Sorption of heavy metals on chitosan-modified biochars and its biological effects. Chemical Engineering Journal. 2013;231:512-8.

21. Ramos V, Rodrıguez N, Rodrıguez M, Heras A, Agullo E. Modified chitosan carrying phosphonic and alkyl groups. Carbohydrate Polymers. 2003;51(4):425-9.

22. Zhang S, Dong Y, Yang Z, Yang W, Wu J, Dong C. Adsorption of pharmaceuticals on chitosan-based magnetic composite particles with core-brush topology. Chemical Engineering Journal. 2016;304:325-34.

23. Krishna B, Murty D, Prakash BJ. Thermodynamics of chromium (VI) anionic species sorption onto surfactant-modified montmorillonite clay. Journal of Colloid and Interface Science. 2000;229(1):230-6.

24. Zhao M, Wu D, Chang J, Bai Z, Jiang K. Synthesis of cup-like ZnO microcrystals via a CTAB-assisted hydrothermal route. Materials Chemistry and Physics. 2009;117(2-3):422-4.

25. Sobeih MM, El-Shahat M, Osman A, Zaid M, Nassar MY. Glauconite clay-functionalized chitosan nanocomposites for efficient adsorptive removal of fluoride ions from polluted aqueous solutions. RSC Advances. 2020;10(43):25567-85.

26. Association APH, Association AWW, Federation WPC, Federation WE. Standard methods for the examination of water and wastewater: American Public Health Association.; 1915.

27. Ahmaruzzaman M, Gayatri SL. Batch adsorption of 4-nitrophenol by acid activated jute stick char: equilibrium, kinetic and thermodynamic studies. Chemical Engineering Journal. 2010;158(2):173-80.

28. Stafiej A, Pyrzynska K. Adsorption of heavy metal ions with carbon nanotubes. Separation and purification technology. 2007;58(1):49-52.

29. Abdelrahman EA, Tolan DA, Nassar MY. A tunable template-assisted hydrothermal synthesis of hydroxysodalite zeolite nanoparticles using various aliphatic organic acids for the

654 removal of zinc (II) ions from aqueous media. Journal of Inorganic and Organometallic Polymers
655 and Materials. 2019;29(1):229-47.

656 30. Smith EH, Lu W, Vengris T, Binkiene R. Sorption of heavy metals by Lithuanian
657 glauconite. Water Research. 1996;30(12):2883-92.

658 31. Li Y, Xu Z, Ma H, S. Hursthouse A. Removal of Manganese(II) from Acid Mine
659 Wastewater: A Review of the Challenges and Opportunities with Special Emphasis on Mn-
660 Oxidizing Bacteria and Microalgae. Water. 2019;11(12):2493.

661 32. Bhatti HN, Nasir AW, Hanif MA. Efficacy of Daucus carota L. waste biomass for the
662 removal of chromium from aqueous solutions. Desalination. 2010;253(1-3):78-87.

663 33. Nassar MY, Mohamed TY, Ahmed IS, Mohamed NM, Khatab M. Hydrothermally
664 synthesized Co 3 O 4, α-Fe 2 O 3, and CoFe 2 O 4 nanostructures: efficient nano-adsorbents for
665 the removal of Orange G textile dye from aqueous media. Journal of Inorganic and Organometallic
666 Polymers and Materials. 2017;27(5):1526-37.

667 34. Dawodu FA, Akpomie KG. Simultaneous adsorption of Ni (II) and Mn (II) ions from
668 aqueous solution unto a Nigerian kaolinite clay. Journal of materials research and technology.
669 2014;3(2):129-41.

670 35. Yavuz Ö, Altunkaynak Y, Güzel F. Removal of copper, nickel, cobalt and manganese from
671 aqueous solution by kaolinite. Water research. 2003;37(4):948-52.

672 36. Ho Y-S. Second-order kinetic model for the sorption of cadmium onto tree fern: A
673 comparison of linear and non-linear methods. Water Research. 2006;40(1):119-25.

674 37. Lagergren S. About the theory of so-called adsorption of soluble substances. Kunglia
675 Svenska Vetenskapsakademiens, Handlingar. 1898;24(4):1-39.

676 38. Yuh-Shan H. Citation review of Lagergren kinetic rate equation on adsorption reactions.
677 Scientometrics. 2004;59(1):171-7.

678 39. Weber WJ, Morris JC. Proceedings of the International Conference on Water Pollution
679 Symposium. Oxford ; New York: Pergamon Press; 1962.

680 40. Nassar MY, Moustafa MM, Taha MM. Hydrothermal tuning of the morphology and
681 particle size of hydrozincite nanoparticles using different counterions to produce nanosized ZnO
682 as an efficient adsorbent for textile dye removal. RSC Advances. 2016;6(48):42180-95.

683 41. Langmuir I. The adsorption of gases on plane surfaces of glass, mica and platinum. Journal
684 of the American Chemical society. 1918;40(9):1361-403.

685 42. Freundlich H. Über die Adsorption in Lösungen. Zeitschrift für Physikalische Chemie: De
686 Gruyter; 1907. p. 385-470.

687 43. Halsey GD. The Role of Surface Heterogeneity in Adsorption. In: W.G. Frankenburg VIK,
688 Rideal EK, editors. Advances in Catalysis. Volume 4: Academic Press; 1952. p. 259-69.

689 44. Alkherraz AM, Ali AK, Elsherif KM. Removal of Pb (II), Zn (II), Cu (II) and Cd (II) from
690 aqueous solutions by adsorption onto olive branches activated carbon: Equilibrium and
691 thermodynamic studies. Chemistry International. 2020;6(1):11-20.

692 45. Anbia M, Amirmahmoodi S. Removal of Hg (II) and Mn (II) from aqueous solution using
693 nanoporous carbon impregnated with surfactants. Arabian Journal of Chemistry. 2016;9:S319-
694 S25.

695 46. Ai L, Zhang C, Liao F, Wang Y, Li M, Meng L, et al. Removal of methylene blue from
696 aqueous solution with magnetite loaded multi-wall carbon nanotube: Kinetic, isotherm and
697 mechanism analysis. Journal of Hazardous Materials. 2011;198:282-90.

698 47. Zhang P, Lo I, O'Connor D, Pehkonen S, Cheng H, Hou D. High efficiency removal of
699 methylene blue using SDS surface-modified ZnFe2O4 nanoparticles. Journal of Colloid and
700 Interface Science. 2017;508:39-48.

701 48. Dubinin M. The potential theory of adsorption of gases and vapors for adsorbents with
702 energetically nonuniform surfaces. Chemical Reviews. 1960;60(2):235-41.

703 49. Onyango MS, Kojima Y, Aoyi O, Bernardo EC, Matsuda H. Adsorption equilibrium
704 modeling and solution chemistry dependence of fluoride removal from water by trivalent-cation-
705 exchanged zeolite F-9. Journal of Colloid and Interface Science. 2004;279(2):341-50.

706 50. Nassar MY, Ahmed IS, Mohamed TY, Khatab M. A controlled, template-free, and
707 hydrothermal synthesis route to sphere-like [small alpha]-Fe2O3 nanostructures for textile dye
708 removal. RSC Advances. 2016;6(24):20001-13.

709 51. Tran HN, You S-J, Hosseini-Bandegharaei A, Chao H-P. Mistakes and inconsistencies
710 regarding adsorption of contaminants from aqueous solutions: A critical review. Water Research.
711 2017;120:88-116.

712 52. Niwas R, Gupta U, Khan AA, Varshney KG. The adsorption of phosphamidon on the
713 surface of styrene supported zirconium (IV) tungstophosphate: a thermodynamic study. Colloids
714 and Surfaces A: Physicochemical and Engineering Aspects. 2000;164(2–3):115-9.

715 53. Milonjić SK. A consideration of the correct calculation of thermodynamic parameters of
716 adsorption. Journal of the Serbian Chemical Society. 2007;72(12):1363-7.

717 54. Khobragade M, Pal A. Investigation on the adsorption of Mn (II) on surfactant-modified
718 alumina: Batch and column studies. Journal of Environmental Chemical Engineering.
719 2014;2(4):2295-305.

720 55. Govindasamy V, Sahadevan R, Subramanian S, Mahendradas DK. Removal of malachite
721 green from aqueous solutions by perlite. International Journal of Chemical Reactor Engineering.
722 2009;7(1).

56. Hao OJ, Tsai CM, Huang CP. The removal of metals and ammonium by natural glauconite. Environment International. 1987;13(2):203-12.

57. Kamal MA, Bibi S, Bokhari SW, Siddique AH, Yasin T. Synthesis and adsorptive characteristics of novel chitosan/graphene oxide nanocomposite for dye uptake. Reactive and Functional Polymers. 2017;110:21-9.

58. Chen N, Zhang Z, Feng C, Li M, Zhu D, Chen R, et al. An excellent fluoride sorption behavior of ceramic adsorbent. Journal of Hazardous Materials. 2010;183(1-3):460-5.

59. Bhatt R, Sreedhar B, Padmaja P. Adsorption of chromium from aqueous solutions using crosslinked chitosan–diethylenetriaminepentaacetic acid. International Journal of Biological Macromolecules. 2015;74:458-66.

60. Bajda T, Kłapyta Z. Adsorption of chromate from aqueous solutions by HDTMA-modified clinoptilolite, glauconite and montmorillonite. Applied Clay Science. 2013;86:169-73.

61. Kuang Y, Zhang X, Zhou S. Adsorption of methylene blue in water onto activated carbon by surfactant modification. Water. 2020;12(2):587.

62. Sayed AS. Removal of toxic pollutants from aqueous solutions by adsorption onto organo-kaolin. Carbon letters. 2009;10(4):305-13.

63. Wef AA. Standard methods for the examination of waterand wastewater. American Public Health Association, AmericanWater Works Association, Water Environmental Federation, 21st Edition, Washington DC, USA. 2005.

64. Taffarel SR, Rubio J. On the removal of Mn2+ ions by adsorption onto natural and activated Chilean zeolites. Minerals Engineering. 2009;22(4):336-43.

65. Üçer A, Uyanik A, Aygün Ş. Adsorption of Cu (II), Cd (II), Zn (II), Mn (II) and Fe (III) ions by tannic acid immobilised activated carbon. Separation and purification technology. 2006;47(3):113-8.

66. bin Jusoh A, Cheng W, Low W, Nora'aini A, Noor MMM. Study on the removal of iron and manganese in groundwater by granular activated carbon. Desalination. 2005;182(1-3):347-53.

67. Adekola F, Hodonou D, Adegoke H. Thermodynamic and kinetic studies of biosorption of iron and manganese from aqueous medium using rice husk ash. Applied Water Science. 2016;6(4):319-30.

68. Rajic N, Stojakovic D, Jevtic S, Logar NZ, Kovac J, Kaucic V. Removal of aqueous manganese using the natural zeolitic tuff from the Vranjska Banja deposit in Serbia. Journal of Hazardous Materials. 2009;172(2-3):1450-7.

69. Shehap A, Bakr A, Hussein OT. Characterization of Clay/Chitosan Nanocomposites and their Use for Adsorption On Mn (II) from Aqueous Solution. International Journal of Science and Engineering Applications. 2015;4.

70. Reiad NA, Salam OEA, Abadir EF, Harraz FA. Adsorptive removal of iron and manganese ions from aqueous solutions with microporous chitosan/polyethylene glycol blend membrane. Journal of Environmental Sciences. 2012;24(8):1425-32.

Highlights

- Adsorptive removal of manganese ions from polluted aqueous media.
- Natural low-cost Egyptian glauconite clay (G) and its modified-chitosan nanocomposites were applied as adsorbents.
- Equilibrium, kinetics, and thermodynamics of manganese adsorption process were studied.
- SDS -CS/G nanocomposite showed the most efficient adsorbents in this study.
- The raw glauconite and its nanocomposites are promising candidates for manganese ions removal from polluted water.

Table 1. Kinetic models calculated parameters for Mn(II) adsorption on G, GL-CS/G, EDTA-GL-CS/G, SDS-CS/G and CTAB-CS/G adsorbents.

Adsorbent	C_0 (mg/L)		Pseudo-first-order			Pseudo-second-order			Intra-particle diffusion		
		$q_{e,(exp)}$ (mg/g)	r^2	k_1 (1/min)	$q_{e,(cal)}$ (mg/g)	r^2	k_2 (g/ (mg min))	$q_{e,(cal)}$ (mg/g)	r^2	k_i (mg/(g $min^{0.5}$)	C (mg/g)
G	50	2.18	0.943	0.008	2.25	1.00	0.15	2.25	0.824	0.011	2.05
GL-CS/G	50	12.67	0.842	0.006	13.30	0.999	0.006	13.35	0.743	0.29	7.79
EDTA-GL-CS	50	16.50	0.900	0.007	17.29	0.999	0.005	17.32	0.736	0.28	12.10
SDS-CS/G	50	17.53	0.906	0.008	17.98	0.999	0.004	18.20	0.831	0.32	12.16
CTAB-CS/G	50	14.18	0.825	0.006	14.82	0.999	0.005	14.80	0.720	0.29	9.43

782

Table 2. Isothermal parameters for Mn(II) ions adsorption onto G, GL-CS/G, EDTA-GL-CS/G, SDS-CS/G, and CTAB-CS/G adsorbents.

Adsorbent	Langmuir isotherm parameters				Freundlich isotherm parameters				D.-R. isotherm parameters			
	$q_{m(exp)}$ (mgg^{-1})	$q_{m(cal)}$ (mgg^{-1})	b (Lmg^{-1})	r^2	$q_{m(cal)}$ (mgg^{-1}) (for C_0= 10-300 mgL^{-1})	K_F ($(mgg^{-1})(Lmg^{-1})^{1/n}$)	n	r^2	q_m (mgg^{-1})	β ($(mgg^{-1})^2$)	E ($kJmol^{-1}$)	r^2
G	3.75	3.74	0.21	0.999	1.77-4.81	0.896	3.39	0.93	2.94	0.15	1.84	0.800
GL-CS/G	24.11	24.60	0.091	0.995	9.98-28.17	5.02	3.23	0.985	18.13	0.36	1.19	0.650
EDTA-GL-CS/G	27.15	28.1	0.125	0.998	14.04-30.49	8.31	4.37	0.984	20.77	0.03	3.79	0.640
SDS-CS/G	27.74	28.46	0.188	0.998	16.24-31.14	10.41	5.18	0.994	22.06	0.02	5.58	0.702
CTAB-CS/G	26.25	27.09	0.082	0.996	10.89-30.83	5.42	3.27	0.987	19.61	0.28	1.32	0.650

Table 3. Dimensionless separation factor (R_L) determined from Langmuir constant (b) for Mn(II) ion adsorption on G, GL-CS/G, EDTA-GL-CS/G, SDS-CS/G and CTAB-CS/G adsorbents.

Initial Mn(II) ion concentration (mgL^{-1})	Dimensionless separation factor (R_L)				
	G	GL-CS/G	EDTA-GL-CS/G	SDS-CS/G	CTAB-CS/G
10	0.322	0.523	0.444	0.347	0.549
20	0.192	0.354	0.285	0.210	0.378
50	0.086	0.180	0.137	0.096	0.196
100	0.045	0.099	0.074	0.050	0.108
150	0.031	0.068	0.051	0.034	0.075
200	0.023	0.052	0.038	0.025	0.057
300	0.018	0.042	0.031	0.021	0.046

Table 4. Thermodynamic parameters for the adsorption of Mn(II) ions on G, GL-CS/G, EDTA-GL-CS/G, SDS-CS/G, and CTAB-CS/G adsorbents.

Adsorbent	T(K)	K_c at different K temperatures					ΔG^o (kJmol^{-1}) at different K temperatures					ΔH^o (kJ/mol)	ΔS^o (kJ/(mol k)
		298	303	308	313	318	298	303	308	313	318		
G		340.6	352.6	353.2	381	391	-14.5	-14.8	-15.03	-15.47	-15.8	5.55	0.07
GL-CS/G		513.8	514	519.6	524.2	527	-15.5	-15.7	-16.0	-16.3	-16.6	1.40	0.06
EDTA-GL-CS/G		970.6	982	1001	1062	1112	-17.1	-17.4	-17.7	-18.1	-18.6	5.50	0.075
SDS-CS/G		1173.3	1185	1196	1222	1236	-17.5	-17.8	-18.1	-18.5	-18.8	2.13	0.07
CTAB-CS/G		654.7	655.3	659.5	667.1	670.4	-16.0	-16.3	-16.6	-17.0	-17.2	1.03	0.057

Table 5. The comparison of maximum adsorption capacities of various materials toward the adsorption of Mn(II) ions.

Adsorbent	**q_{max} (mg/g)**	**Reference**
kaolinite clay	0.45	(35)
Activated zeolite with NaCl	0.78	(64)
Activated carbon immobilized by tannic acid	1.73	(65)
Granular Activated carbon	2.54	(66)
Rice husk	3.21	(67)
Glauconite (G)	3.75	Present study
Zeolite	6.96	(68)
Montmorillonite chitosan biocomposite (MMT)	10.11	(69)
Chitosan/polyethylene glycol blend membrane	21.70	(70)
Modified Chitosan-glauconite composite (GL-CS/G)	24.11	Present study
CTAB-modified glauconite (CTAB-CS/G)	26.25	Present study
EDTA-modified glauconite (EDTA-GL-CS/G)	27.15	Present study
SDS-modified glauconite (SDS-CS/G)	27.74	Present study
CTAB-treated mesoporous carbon adsorbent	43.0	(45)
SDS- treated mesoporous carbon adsorbent	47.0	(45)

Table 6. Physico-chemical parameters of real wastewater sample after its treatment using the as-prepared adsorbents.

Water quality parameters	Content (mg/L)	
	Before treatment	After treatment (The obtained range for applying G clay and its composites)
pH	3.12	6-6.5
Electrical Conductivity (µm/cm)	9060	71.25-85.77
Turbidity (NTU)	51.00	90.00-98.00%
Total Hardness (mg/L)	3100	90.00-93.84.00%
COD	180	80.00-84.00%
P (mg/L)	1800	88.00-90.10%
T.S (mg/L)	16500	61.15-70.20%
T.D.S (mg/L)	13300	51.00-55.80%
T.S.S (mg/L)	3200	72.11-66.22%
CL (mg/L)	369.2	66.41-72.33 %
Fe (mg/L)	518	96.12-97.87%
Na (mg/L)	610	83.20-86.10%
K (mg/L)	150	68.80-74.80%
S (mg/L)	3500	88.84-92.11%
Mg (mg/L)	190.10	87.10-90%
Mn (mg/L)	18.06	94.10-82.42%

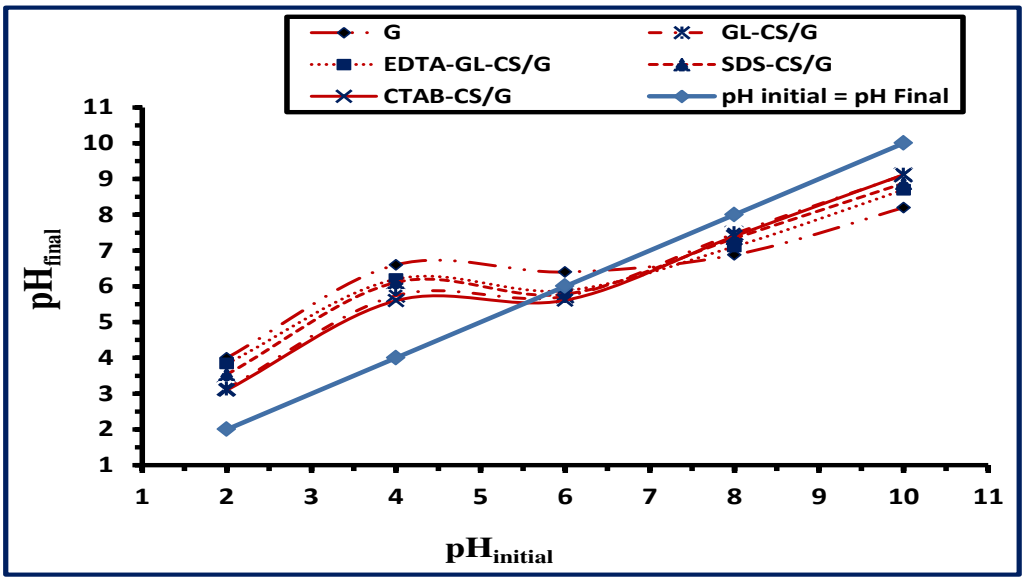

Fig.1. Determination of the point zero charge values of G, GL-CS/G, EDTA-GL-CS/G, SDS-CS/G, and CTAB-CS/G adsorbents.

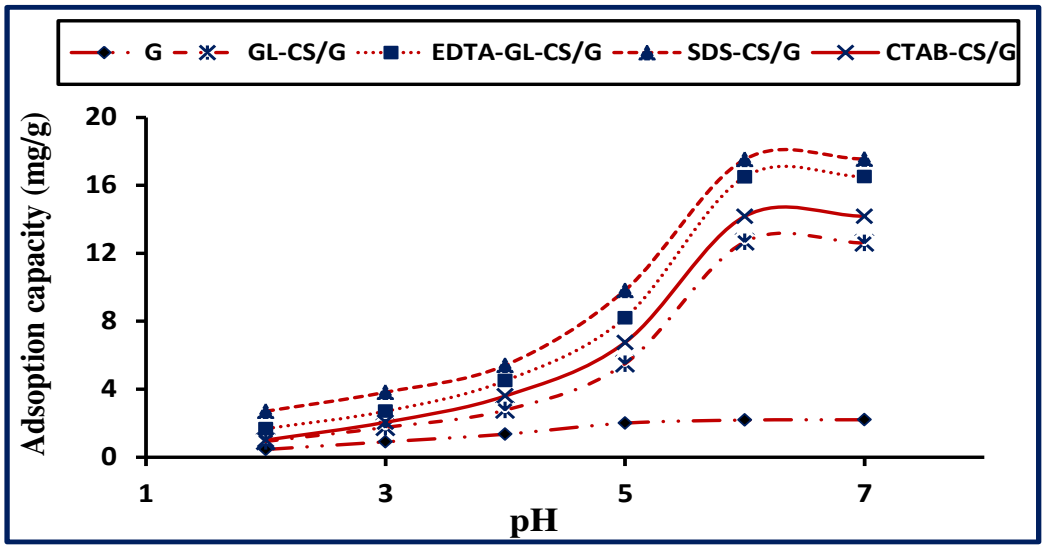

Fig.2. Effect of pH values on Mn(II) adsorption onto G, GL-CS/G, EDTA-GL-CS/G, SDS-CS/G, and CTAB-CS/G adsorbents.

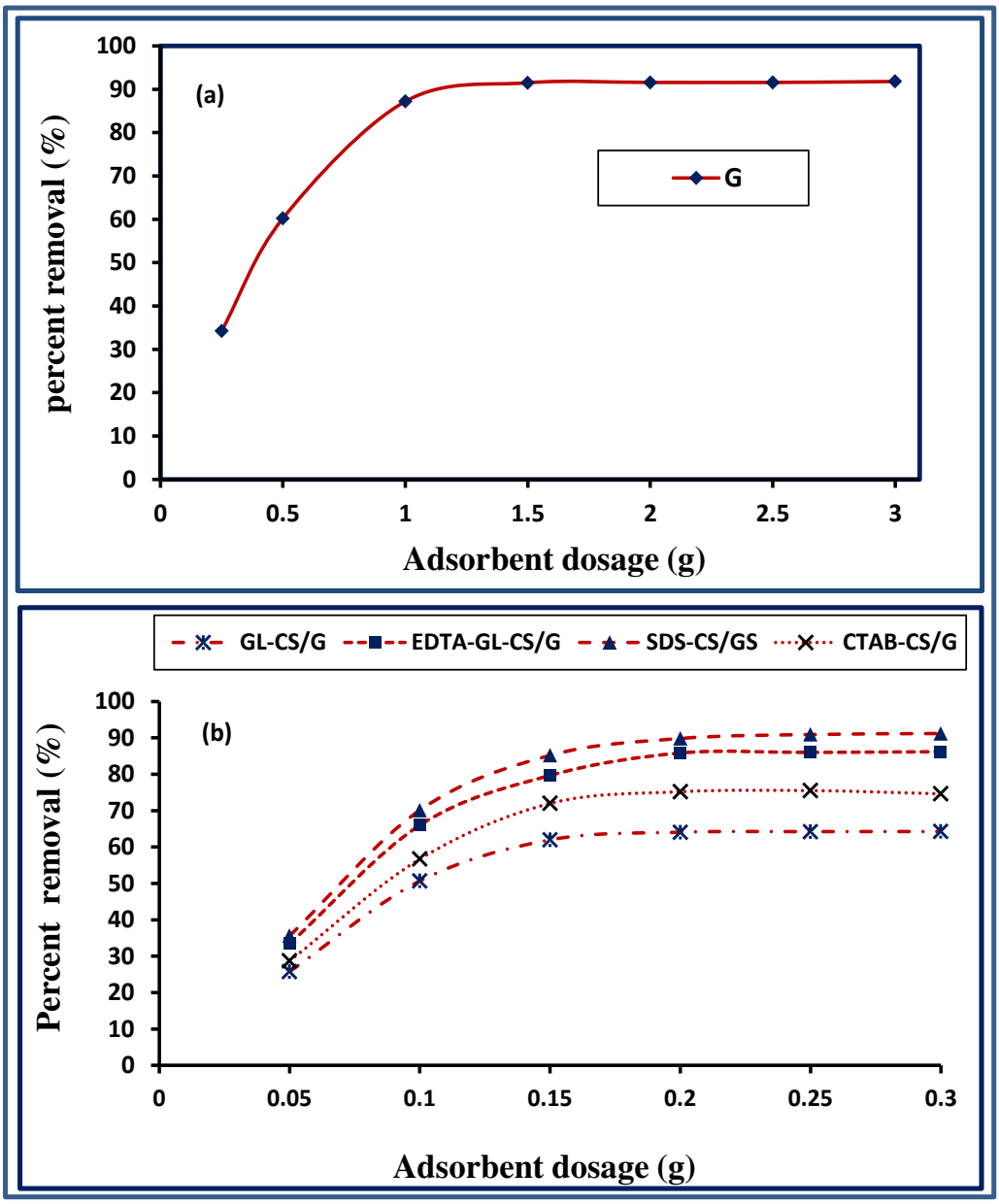

Fig. 3. Influence of adsorbent dosage on Mn(II) ions removal using G (a); GL-CS/G, EDTA-GL-CS/G, SDS-CS/G, and CTAB-CS/G (b) adsorbents.

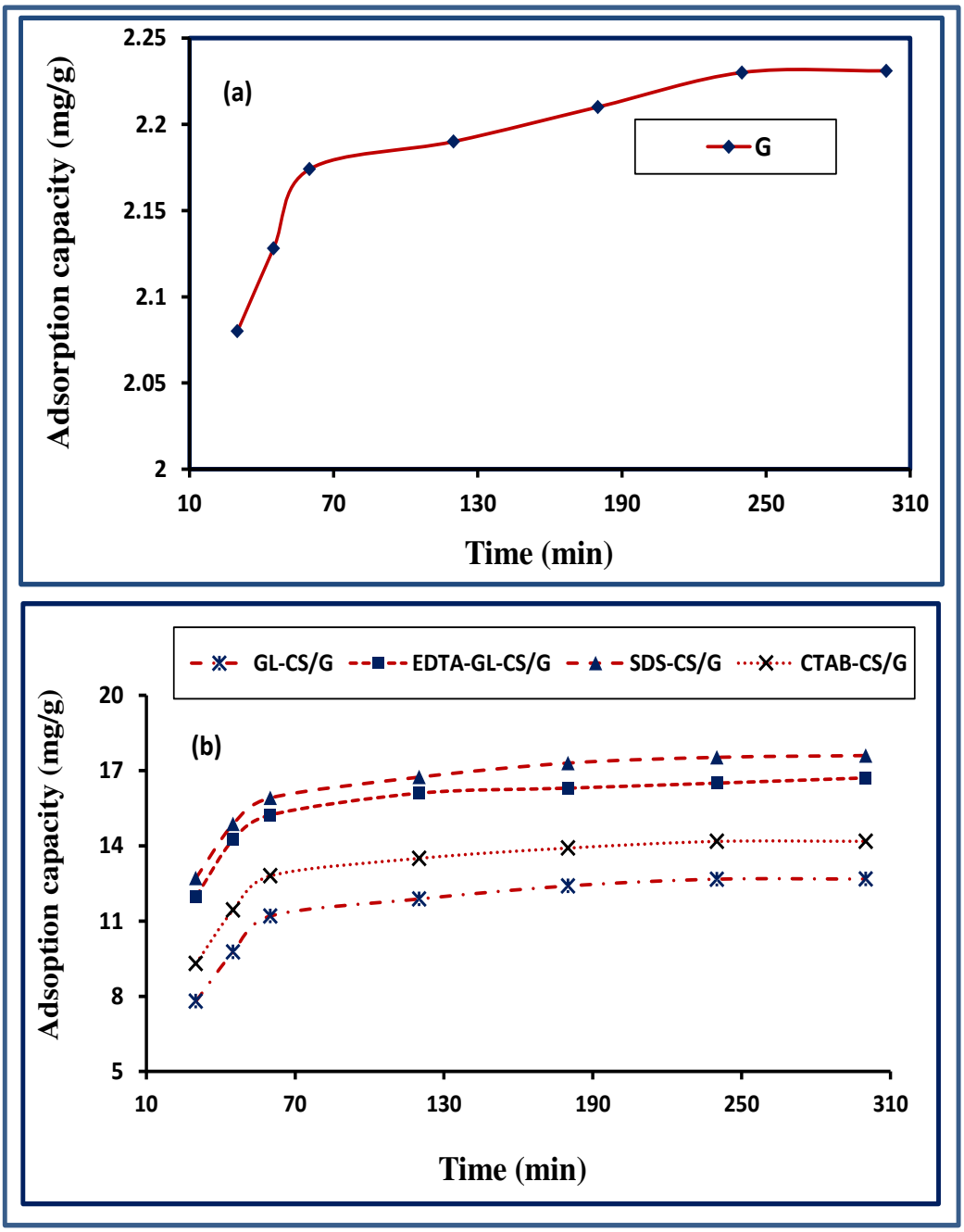

Fig. 4. Influence of contact time on Mn(II) ions adsorption capacity using G (a); GL-CS/G, EDTA-GL-CS/G, SDS-CS/G, and CTAB-CS/G (b) adsorbents.

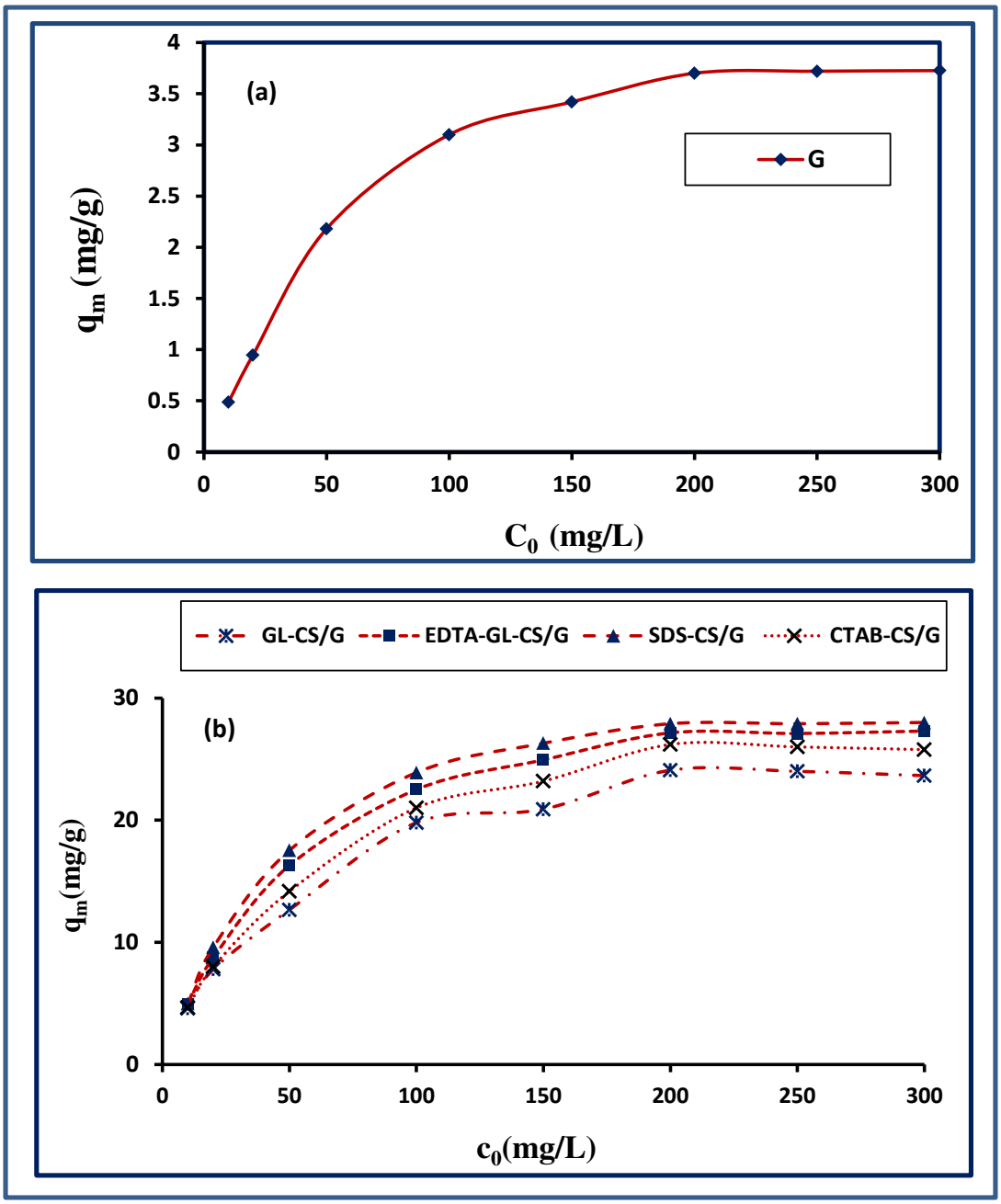

Fig. 5. Influence of initial Mn(II) ions concentration on adsorption capacity of G (a); GL-CS/G, EDTA-GL-CS/G, SDS-CS/G, and CTAB-CS/G (b) adsorbents.

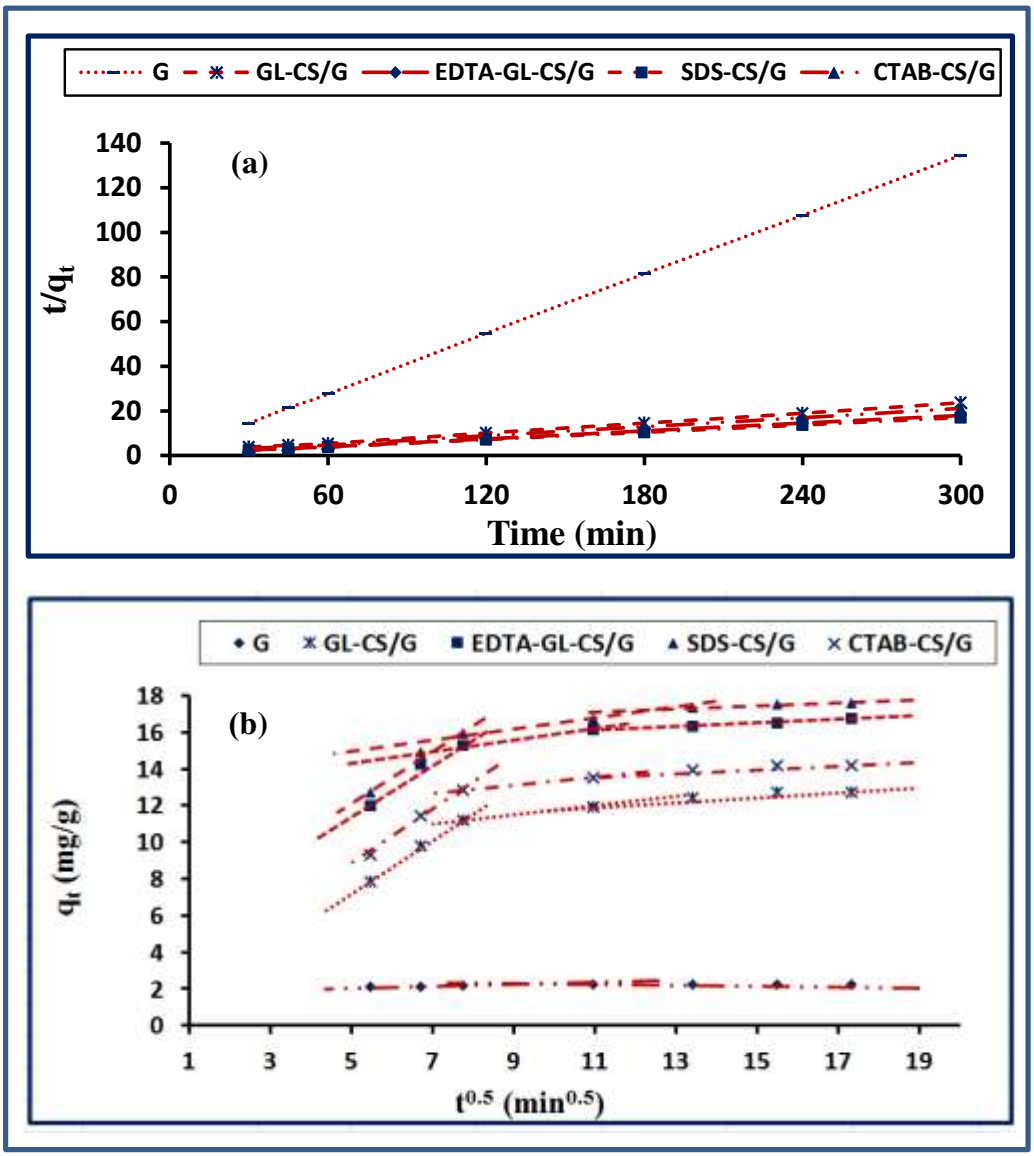

Fig. 6. Pseudo-second-order kinetic model (a), and validation of intra-particle-diffusion model (b) for Mn(II) ions adsorption onto G, GL-CS/G, EDTA-GL-CS/G, SDS-CS/G, and CTAB-CS/G adsorbents.

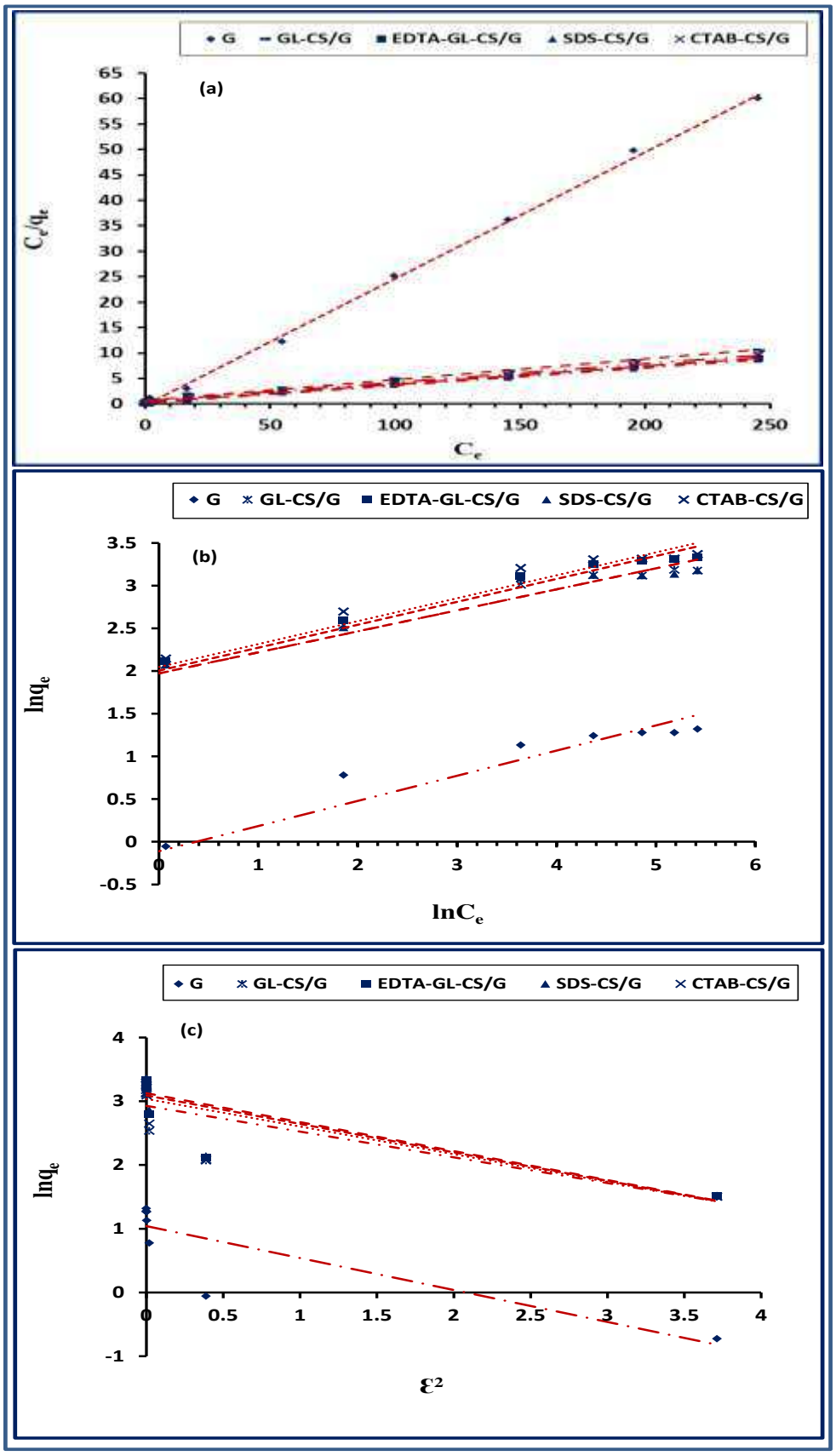

Fig. 7. Adsorption isotherms of Mn(II) ions onto G, GL-CS/G, EDTA-GL-CS/G, SDS-CS/G, and CTAB-CS/G adsorbents: Langmuir (a), Freundlich (b), and Dubinin-Radushkevich (c).

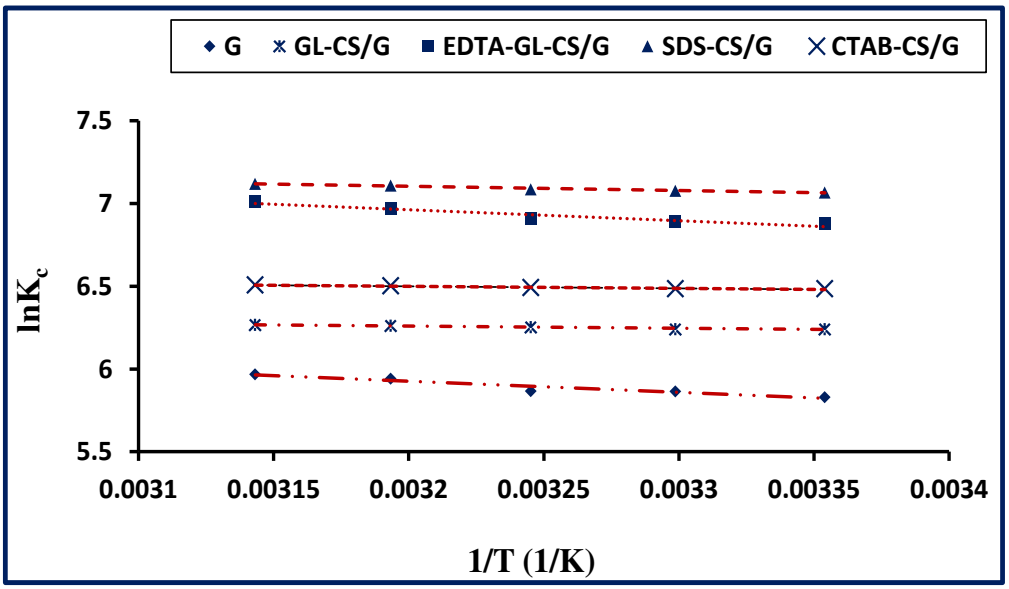

Fig. 8. The plots of $\ln K_C$ versus 1/T for Mn(II) ions removal using G, GL-CS/G, EDTA-GL-CS/G, SDS-CS/G, and CTAB-CS/G adsorbents

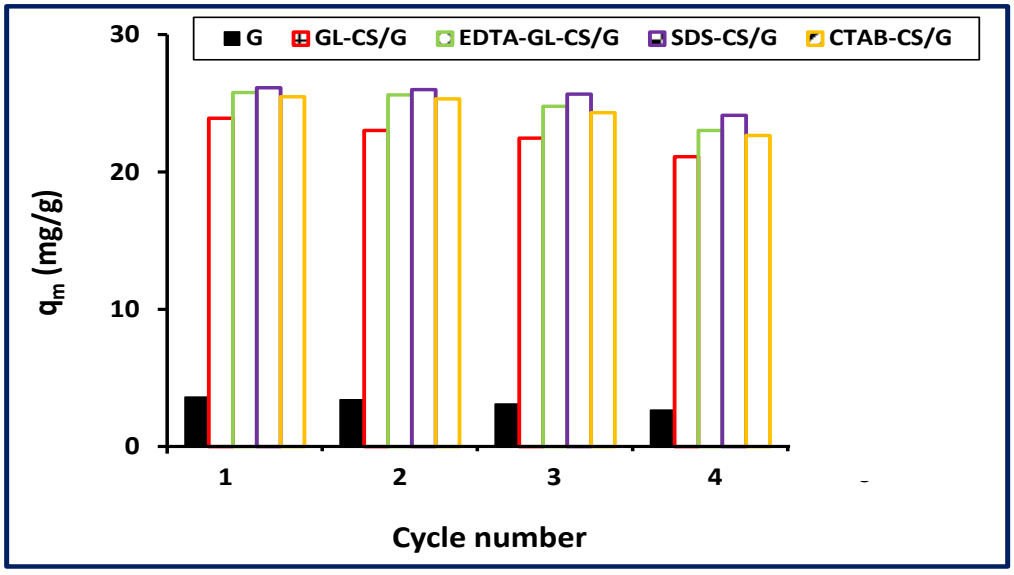

Fig. 9. Regeneration efficiency of G, GL-CS/G, EDTA-GL-CS/G, SDS-CS/G, and CTAB-CS/G adsorbents for Mn(II) ion adsorption from aqueous media.

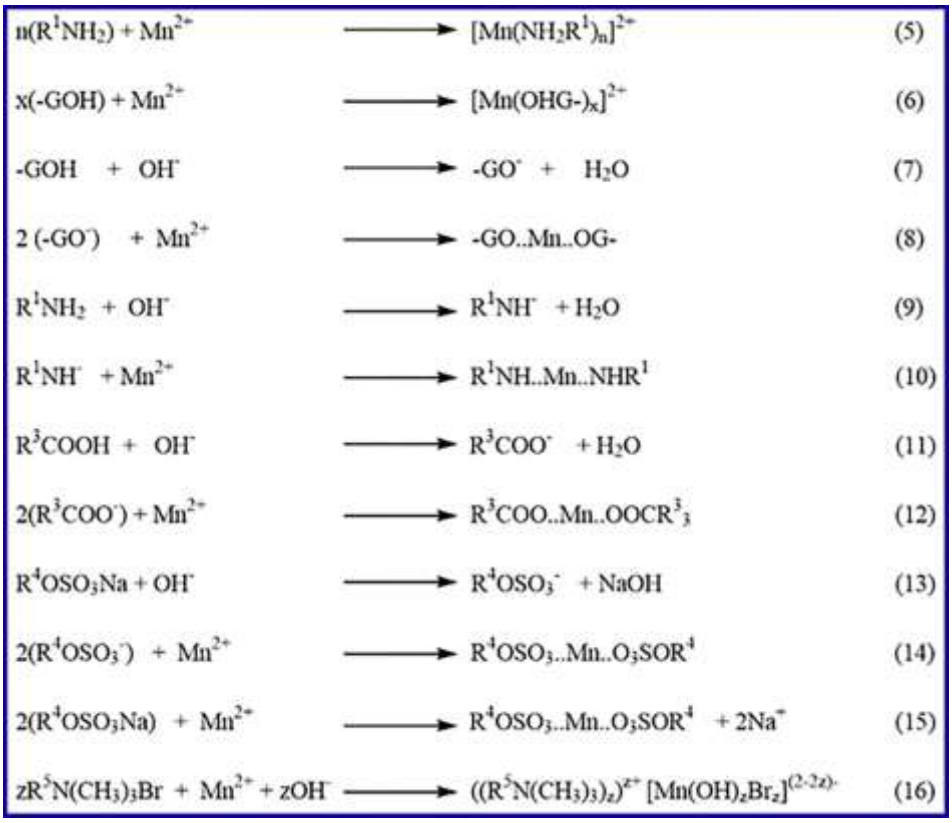

Scheme 1. Suggested adsorption mechanism of Mn(II) ions onto G, GL-CS/G, EDTA-GL-CS/G, SDS-CS/G, and CTAB-CS/G adsorbents. Where R^1, R^2, R^3, R^4, and R^5 represent the aliphatic groups in the modified chitosan nanocomposites.

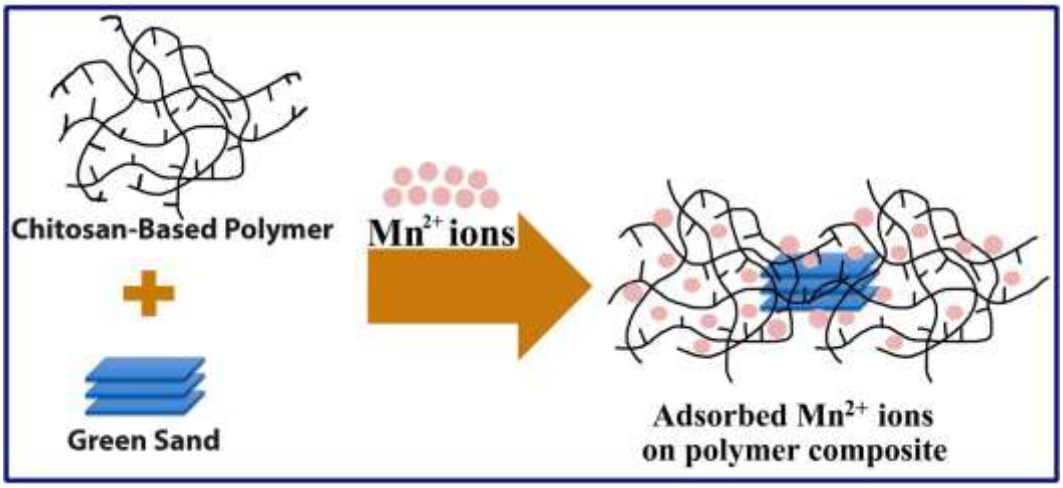

Graphical Abstract

Figures

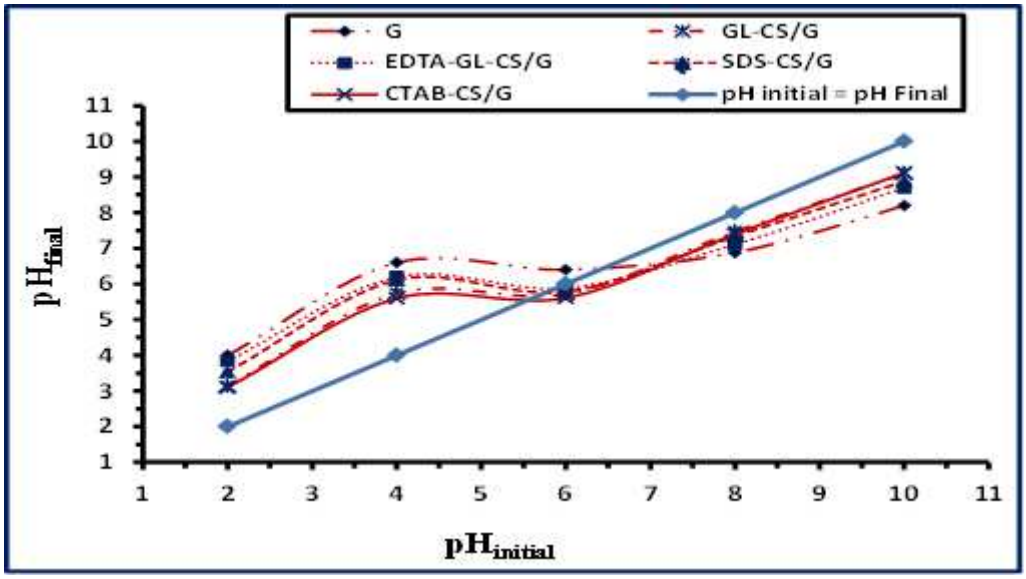

Figure 1

Determination of the point zero charge values of G, GL-CS/G, EDTA-GL-CS/G, SDS-CS/G, and CTAB-CS/G adsorbents.

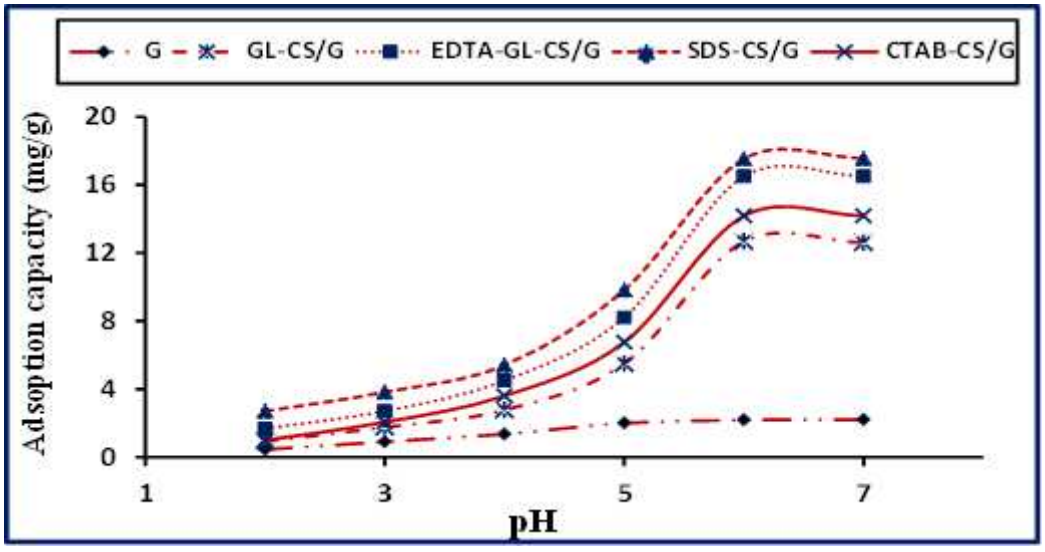

Figure 2

Effect of pH values on Mn(II) adsorption onto G, GL-CS/G, EDTA-GL-CS/G, SDS-CS/G, and CTAB-CS/G adsorbents.

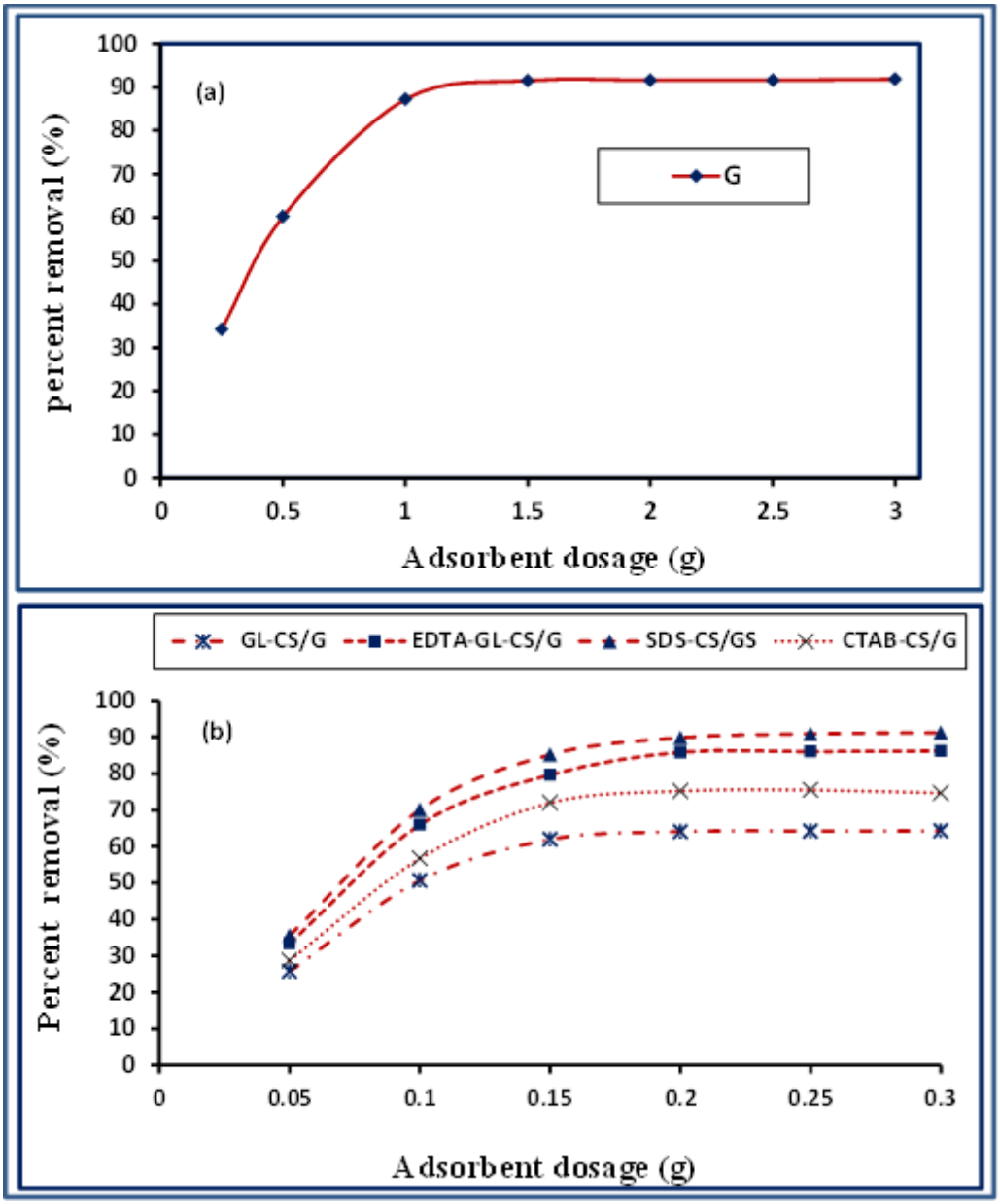

Figure 3

Influence of adsorbent dosage on Mn(II) ions removal using G (a); GL-CS/G, EDTA-GL-CS/G, SDS-CS/G, and CTAB-CS/G (b) adsorbents.

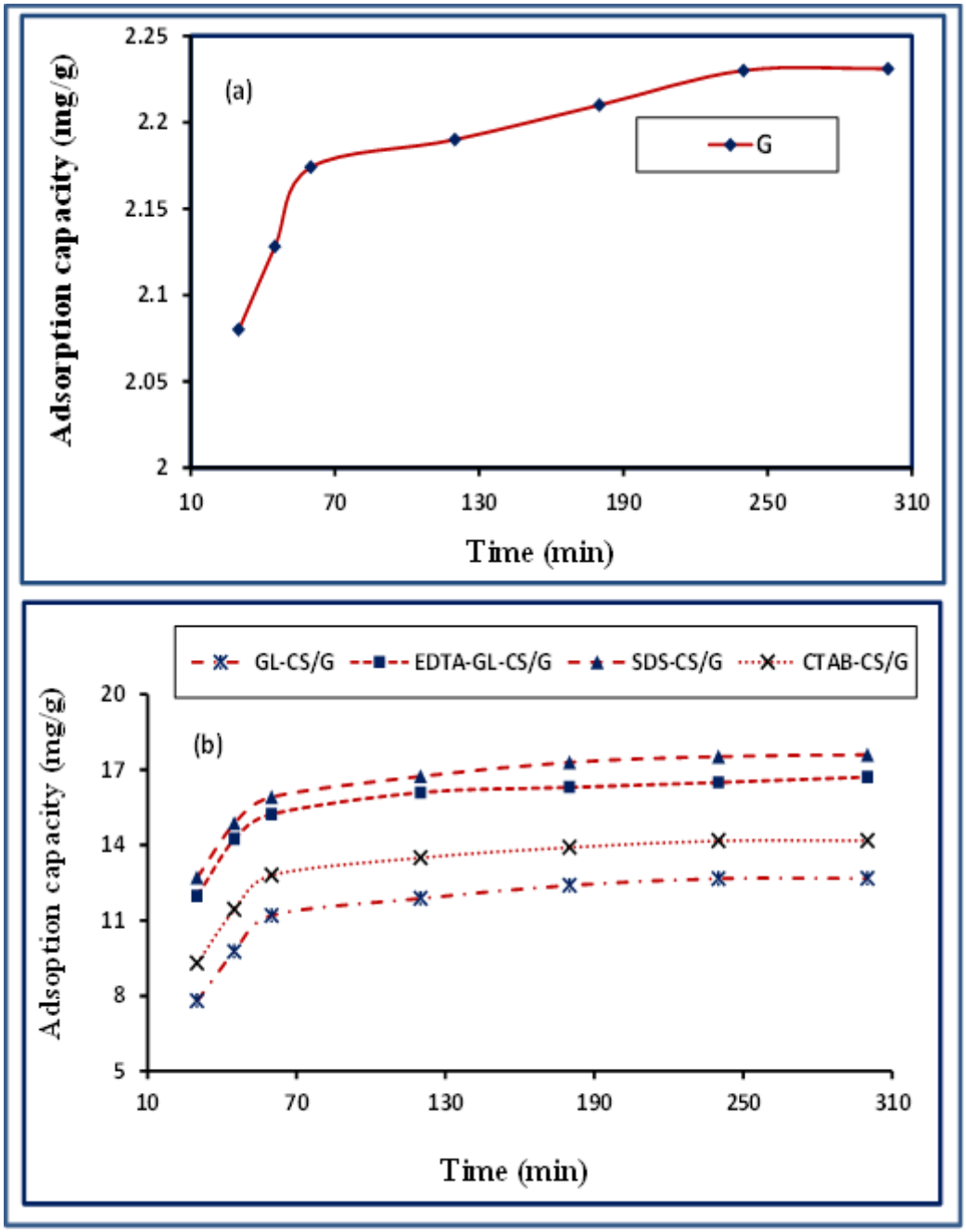

Figure 4

Influence of contact time on Mn(II) ions adsorption capacity using G (a); GL-CS/G, EDTA-GL-CS/G, SDS-CS/G, and CTAB-CS/G (b) adsorbents.

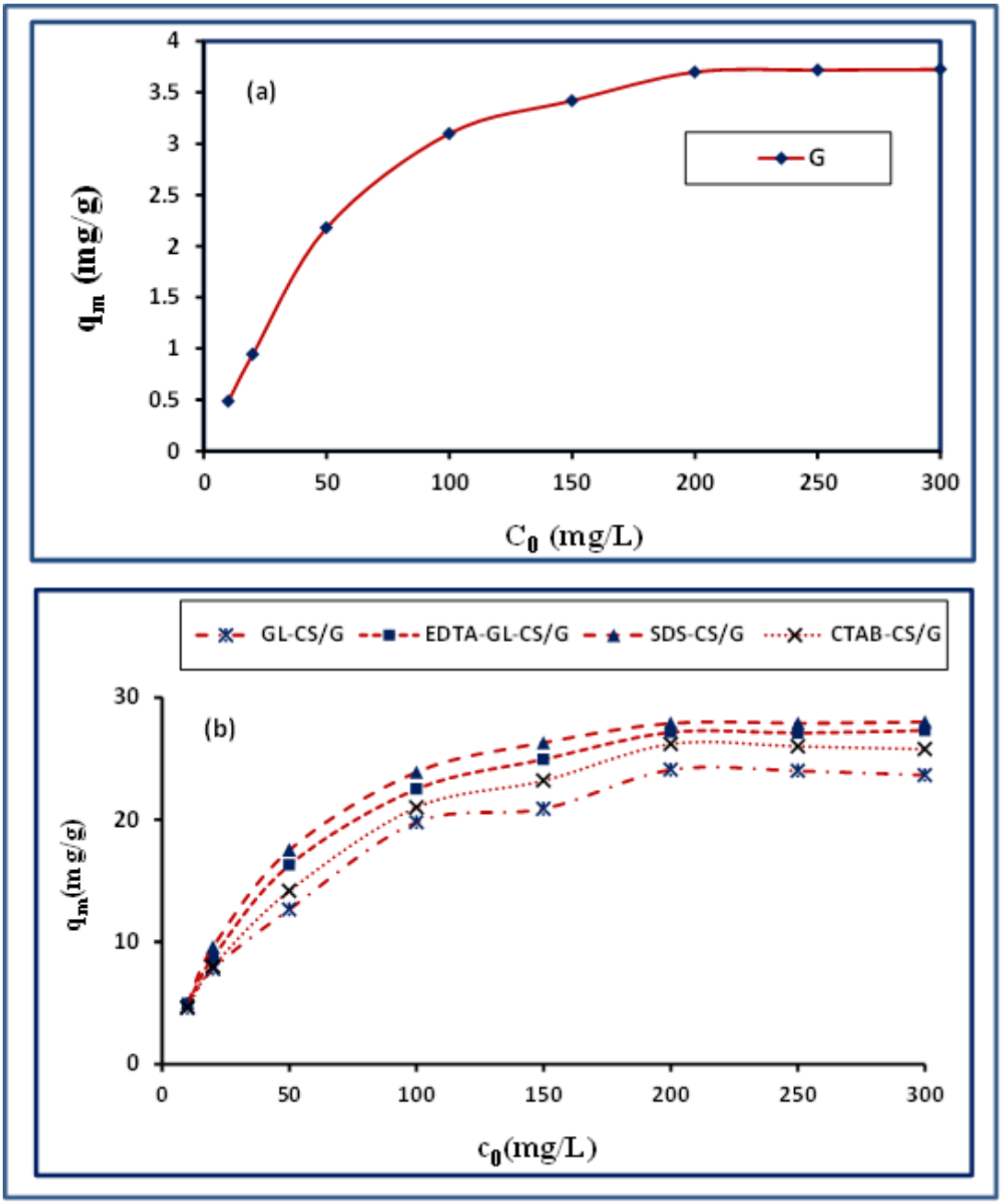

Figure 5

Influence of initial Mn(II) ions concentration on adsorption capacity of G (a); GL-CS/G, EDTA-GL-CS/G, SDS-CS/G, and CTAB-CS/G (b) adsorbents.

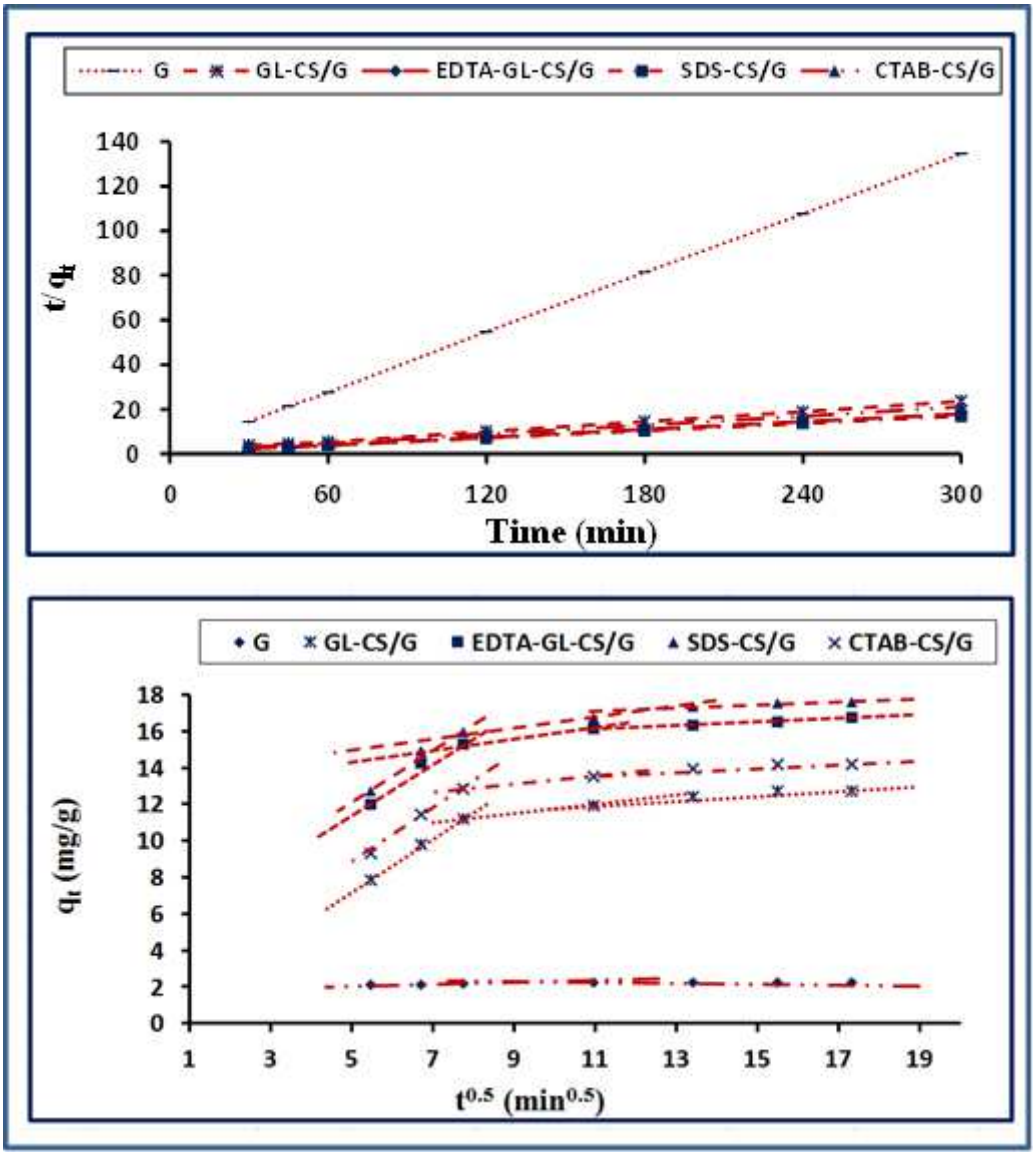

Figure 6

Pseudo-second-order kinetic model (a), and validation of intra-particle-diffusion model (b) for Mn(II) ions adsorption onto G, GL-CS/G, EDTA-GL-CS/G, SDS-CS/G, and CTAB-CS/G adsorbents.

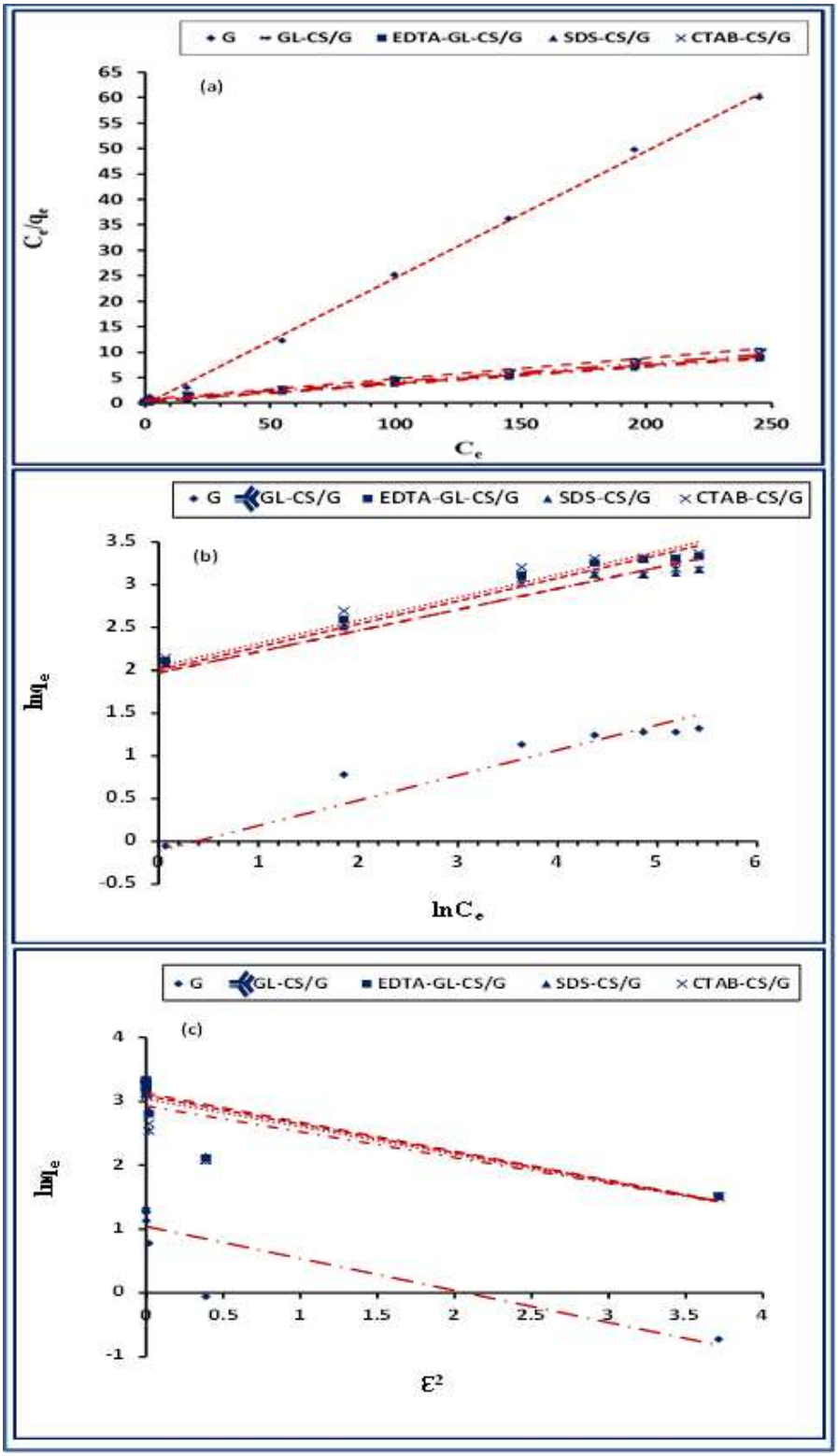

Figure 7

Adsorption isotherms of Mn(II) ions onto G, GL-CS/G, EDTA-GL-CS/G, SDS-CS/G, and CTAB-CS/G adsorbents: Langmuir (a), Freundlich (b), and Dubinin-Radushkevich (c).

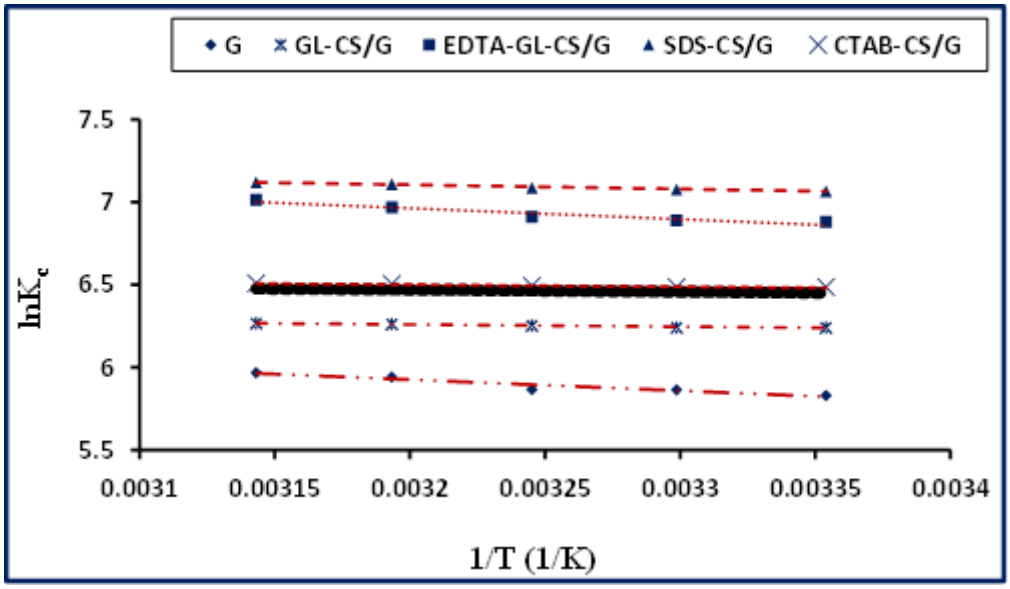

Figure 8

The plots of lnKC versus 1/T for Mn(II) ions removal using G, GL-CS/G, EDTA-GL-CS/G, SDS-CS/G, and CTAB-CS/G adsorbents

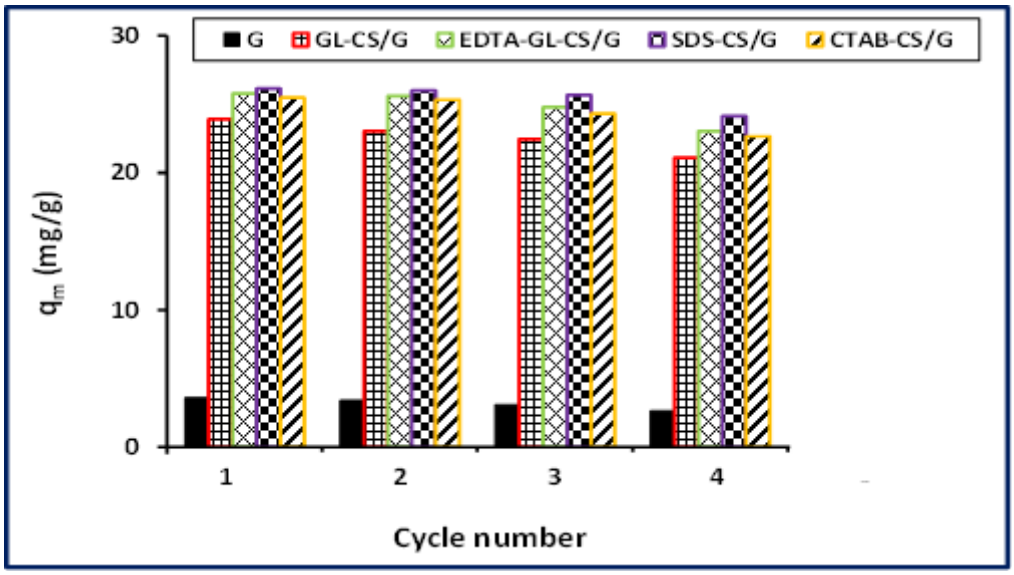

Figure 9

Regeneration efficiency of G, GL-CS/G, EDTA-GL-CS/G, SDS-CS/G, and CTAB-CS/G adsorbents for Mn(II) ion adsorption from aqueous media.

Supplementary Files

This is a list of supplementary files associated with this preprint. Click to download.

- Scheme01.png

- GA.png